# Casein kinase 1δ-regulated formation of GVBs induces resilience to tau pathology-mediated protein synthesis impairment

Jasper F.M. Smits[1,2], Thijmen W. Ligthart[1], Marta Jorge-Oliva[2], Skip Middelhoff[1,2], Fleur Schipper[2], Renee Garritsen[2], Débora Pita-Illobre[3], Ka Wan Li[3] and Wiep Scheper[1,2*]

[1]Dept. of Human Genetics, Amsterdam UMC - Vrije Universiteit Amsterdam, The Netherlands; [2]Dept. of Functional Genomics and [3]Dept. of Molecular and Cellular Neuroscience, Center for Neurogenomics and Cognitive Research, Amsterdam Neuroscience, Vrije Universiteit Amsterdam, The Netherlands

**Keywords**: granulovacuolar degeneration bodies (GVBs), tau pathology, Casein kinase 1δ, proteostasis

*Correspondence to:
Wiep Scheper
Research Building Vrije Universiteit Amsterdam
Center for Neurogenomics and Cognitive Research
Department of Functional Genomics
De Boelelaan 1100
1081 HZ Amsterdam
The Netherlands
w.scheper@amsterdamumc.nl

**Abstract**

In Alzheimer's disease, many surviving neurons with tau pathology contain granulovacuolar degeneration bodies (GVBs), neuron-specific lysosomal structures induced by pathological tau assemblies. This could indicate a neuroprotective role for GVBs, however, the mechanism of GVB formation and its functional implications are elusive. Here, we demonstrate that GVB formation depends on CK1δ activity and basal autophagy. We show that neurons with GVBs (GVB+) are resilient to tau-induced impairment of global protein synthesis and are protected against tau-mediated neurodegeneration. GVB+ neurons have multiple adaptations to counteract the tau pathology-induced decline in protein synthesis, including increased ribosomal content. Importantly, unlike neurons without GVBs, GVB+ neurons fully retain the capacity to induce long-term potentiation-induced protein synthesis in the presence of tau pathology. Our results have identified CK1δ as a key regulator of GVB formation that confers a protective neuron-specific proteostatic stress response to tau pathology. Our findings provide novel opportunities for targeting neuronal resilience in tauopathies.

## Main

The progressive intraneuronal accumulation of aggregated proteins is central in the pathogenesis of neurodegenerative diseases, with tau protein in Alzheimer's disease (AD) and frontotemporal dementias (FTD) as a prime example[1]. Neurons depend on robust protein homeostasis (proteostasis) to acquire and maintain properties required for neuronal function. Moreover, post-mitotic neurons cannot self-renew and their unique features that are acquired throughout their lifetime make them difficult to replace. Pathological tau accumulation impairs neuronal protein synthesis[2–6], thereby strongly challenging proteostasis. Consequently, neurons must possess intrinsic mechanisms to withstand proteostatic disturbances. Granulovacuolar degeneration bodies (GVBs) are membrane-delineated structures that accumulate in the soma of a subset of neurons affected by early stages of tau pathology[7–9], yet their functional role in tau pathogenesis remains unclear. The high number of GVB+ neurons in brains of cognitively healthy centenarians[10,11] and the observation that the majority of surviving neurons in the AD hippocampus have GVBs[12], suggest that the presence of GVBs may signify a protective proteostatic response. It has been hypothesized that GVBs may protect neurons by sequestering damaging proteins[9,12,13]. Alternatively, the direct connection with pathological tau accumulation could suggest that GVBs function to enhance tau degradation to restore proteostasis. However, there is no convincing evidence for the accumulation of tau in GVBs[13,14], raising the possibility that GVBs affect neurons via an alternative mechanism. Here, we investigated the formation and functional significance of GVBs to elucidate the molecular pathways underlying neuronal resilience to pathological tau-induced proteostatic disturbance.

GVBs were merely enigmatic appearances in *post-mortem* human brain tissue, until our lab recently developed experimental models of tau-induced GVB formation that allow mechanistic study[14–16]. We have demonstrated that the formation of GVBs is a neuron-specific response that is triggered by intraneuronal pathological protein assemblies[14,15]. GVBs are proteolytically active lysosomal structures that contain endo- and autosomal cargo, accumulated in one or multiple dense cores[14]. These cores are strongly immunopositive for several epitopes, including phosphorylated protein kinase R (PKR)-like endoplasmic reticulum kinase (pPERK)[13], that are useful as markers to detect GVBs. However, it is largely unknown whether the immunopositivity of the GVB core reflects the presence of specific proteins or just protein fragments or neo-epitopes (extensively reviewed before[9,13]). To date, the serine/threonine protein kinase casein kinase 1δ (CK1δ) is the only protein validated to selectively accumulate in GVBs using direct fluorescence[14]. However, the mechanism of the formation of GVBs and the potential functional involvement of CK1δ therein is completely unknown.

In the present work, we demonstrate that neurons with GVBs (GVB+ neurons) are more resilient to pathological tau-mediated neurodegeneration. We identified CK1δ activity as a rate-limiting factor in the formation of GVBs and showed that GVB formation requires the autophagic machinery. Neurons with GVBs have an increase in lysosomal and ribosomal content and are resilient to tau-induced impairment of global protein synthesis. Importantly, GVB+ neurons are resilient to the associated impairment of long-term potentiation (LTP)-regulated protein synthesis. Our results demonstrate that GVB formation protects neurons against the proteostatic disturbance induced by tau pathology.

## Results

### GVB+ neurons are resilient to tau-induced neurodegeneration

To study the formation of GVBs in relation to tau pathology over time, we employed our extensively characterized and validated primary neuron model for seed-independent tau pathology where lentiviral transduction with FTDtau$^{1+2}$ (2N4R human tau with the P301L/S320F FTD mutations) results in progressive pathological tau accumulation accompanied by GVB formation[15,16] (Fig.1a). Like GVBs observed in the human brain, these GVBs contained a core positive for CK1δ- and pPERK (Fig.1b) delineated by a lysosomal membrane (Fig.1c) as previously shown[15]. 15 days after FTDtau$^{1+2}$-transduction, around 10% of the neurons with pathological tau assemblies have formed GVBs[15,16] (tau+/GVB+ neurons). At this point, neuronal loss or degeneration of neurites or synapses was not observed (Extended Data Fig.1a-g), and calcium imaging analysis showed that neuronal network activity was unaffected (Extended Data Fig.1h-o), indicating that this timepoint represents a stage in tau pathogenesis that precedes neurodegeneration. However, exposure to tau pathology for an additional week (Fig.1d) induced neuronal loss (Fig.1e). In line with studies in human brain[12], this demonstrated that in contrast to the loss of GVB-negative (GVB-) neurons as tau pathology progresses (Fig.1f), the number of GVB+ neurons increased (Fig.1g), identifying GVB+ neurons as more resilient to tau-induced neurodegeneration. To study the temporal dynamics of GVB formation, the percentage of GVB+ neurons was determined at different incubation periods with FTDtau$^{1+2}$ (Fig.1h, i). While the accumulation of MC1- and AT8-positive tau assemblies started to plateau after 22 days of exposure to FTDtau$^{1+2}$, the number of GVB+ neurons continued to increase up to 35% after 29 days (Fig.1i, j and Extended Data Fig.1p, q). These findings highlight that GVB formation progresses whereas GVB- neurons are lost to tau aggregation, suggesting that GVBs play an adaptive role in neuronal resilience to tau-induced neurodegeneration.

### GVB formation requires basal autophagy

Since lysosomal dysfunction is a hallmark of tauopathies[17,18] and GVBs are lysosomal structures, we investigated whether tau aggregation alters lysosomal characteristics by quantifying lysosomal organelles per neuron using high-resolution confocal microscopy. FTDtau$^{1+2}$-transduced (tau+) neurons displayed fewer and smaller lysosomal organelles than untransduced (tau-) neurons (Fig.2a-c), indicating that intraneuronal tau pathology reduces the lysosomal content. Comparison of tau+/GVB+ to tau+/GVB- neurons showed that GVB+ neurons have more lysosomal organelles, whereas the organelle volume is not different (Fig.2d-f). These findings suggest that GVB+ neurons are resilient to the tau-induced reduction in lysosomal content.

131 Tau aggregation induces the formation of GVBs, however, in line with previous data from the
132 human brain and experimental models (reviewed previously[9,13]), pathological tau does not
133 accumulate in GVBs (Fig.1a). This was not affected by inhibition of lysosomal degradation
134 using E64D and Pepstatin A (Fig.2g), excluding that tau is rapidly degraded in the GVBs. In
135 addition, whereas intraneuronal tau pathology was positive for the aggregate-binding dye
136 Proteostat, no positive signal was observed in GVBs (Fig.2h). Despite the increased lysosomal
137 content in GVB+ neurons, this suggests that GVBs do not play a key role in pathological tau
138 degradation. This prompted us to investigate the broader role of the endo-autolysosomal
139 system in GVB formation. To test the role of endocytosis, tau+ neurons were treated with
140 Filipin3 or Dyngo-4a. This resulted in inhibition of lipid raft- and dynamin-mediated
141 endocytosis, respectively (Extended Data Fig.2a, b). In contrast, the number of GVB+ neurons
142 was not affected, indicating that endocytosis is not required for GVB formation (Extended Data
143 Fig.2c). To explore the role of autophagy, tau+ neurons were treated with Sar405 to block
144 VPS34 (Fig.2i and Extended Data Fig.3a). This efficiently inhibited autophagic flux, as
145 indicated by strongly increased levels of P62 (Extended Data Fig.3b). In addition, the number
146 of GVB+ neurons gradually decreased over time down to 22% of control after 8d treatment
147 (Fig.2i, j). To further support the involvement of autophagy in GVB formation, knock-down
148 (KD) of *Fip200* and *Atg5*, that act after autophagy initiation, was performed (Extended Data
149 Fig.3a). *Fip200* as well as *Atg5* shRNAs[19,20] efficiently reduced the protein levels of their
150 targets (Extended Data Fig.3c, d, f, g) and both increased P62 levels (Extended Data Fig.3e,
151 h), showing inhibition of autophagy. All shRNAs reduced the number of GVB+ neurons
152 (*shFip200* to 38% and *shAtg5* to 25% of control) (Fig.2k-n). To test the effect of activation of
153 autophagy, we employed the mTOR inhibitors Torin1 and rapamycin for 48h (Extended Data
154 Fig.3a). Both treatments strongly reduced 4E-BP1 phosphorylation, showing efficient inhibition
155 of mTOR activity (Extended Data Fig.3i, k). In contrast, the number of GVB+ neurons was not
156 affected by either treatment (Extended Data Fig.3j, l). Together, these results demonstrate
157 that GVB formation is dependent on the autophagic machinery and flux but is not stimulated
158 by increasing autophagic activity.
159

160 **CK1δ activity is a key regulator of GVB formation**

161 To investigate the molecular mechanism associated with the formation of GVBs, the kinase
162 CK1δ is a prime candidate because it selectively accumulates in GVBs[14]. To study the role of
163 CK1δ, tau+ neurons were treated with the CK1δ/ε-specific ATP-competitive kinase inhibitor
164 PF670462[21,22] ($CK1\delta_i$). We studied the effect of $CK1\delta_i$ 15 days after FTDtau[1+2]-transduction.
165 $CK1\delta_i$ treatment was initiated either before or after the first GVBs are detected at day 13[15]
166 (Fig.3a, b). $CK1\delta_i$ did not induce toxicity or negatively affect neuronal morphology or synapse

167 number (Extended Data Fig.4a-m). Using pPERK as a GVB marker, we found that CK1$\delta_i$
168 treatment for 48h or 8d reduced the number of GVB+ neurons to 32% and 3% of control,
169 respectively (Fig.3a, c). This shows that the formation of GVBs is reduced by CK1$\delta_i$ when
170 initiated before or during the first GVBs occur. In contrast, CK1$\delta_i$ treatment for 24h or less did
171 not significantly change the number of GVB+ neurons (Fig.3a, c). To test if this was due to the
172 shorter incubation period or if CK1$\delta_i$ has no effect once GVB formation is in progress, tau
173 pathology exposure was extended to 22 days, with treatment starting well after the onset of
174 GVB formation (Extended Data Fig.4n). The number of GVB+ neurons was also strongly
175 reduced upon CK1$\delta_i$ treatment after 48h (63% of control) and 8d (12% of control) (Extended
176 Data Fig.4o), indicating that CK1δ is required both for the initiation and progression of GVB
177 formation. To exclude that the effect of CK1$\delta_i$ was due to altered phosphorylation of GVB-
178 cargo that may affect the detection of phospho-epitopes like pPERK, we tested the effect of
179 CK1$\delta_i$ using a non-phospho GVB marker that has been identified in AD post-mortem brain,
180 GOLGINA4[23,24]. GOLGINA4 was validated as a bona fide GVB marker in our experimental
181 model as well (Extended Data Fig.5a, b). CK1$\delta_i$ treatment strongly reduced GOLGINA4-
182 detected GVB+ neurons to 30% of control (Extended Data Fig.5c), confirming that CK1$\delta_i$
183 decreases GVB formation. CK1δ is reported to phosphorylate tau *in vitro*[25,26], therefore we
184 assessed pathological tau accumulation as previously described[15,16,27]. Treatment with CK1$\delta_i$
185 for 48h or 8d did not affect the level of MC1-positive FTDtau$^{1+2}$ accumulation (Extended Data
186 Fig.5d, f) and the phospho-epitope-independent direct fluorescence intensity of MeOH-
187 insoluble FTDtau$^{1+2}$-GFP (Extended Data Fig.5e, g). This indicates that the effect of inhibition
188 of CK1δ activity on the number of GVB+ neurons is not caused by an indirect effect on tau
189 pathology. Together, these data place CK1δ upstream in the pathway driving GVB formation.
190
191 To further confirm the key role of CK1δ in GVB generation, shRNA-mediated KD was
192 employed to reduce CK1δ protein levels (Extended Data Fig.6a-c). *shCsnk1d* significantly
193 reduced the percentage of GVB+ neurons to 52% of control (Extended Data Fig.6d, e).
194 Because of the high toxicity associated with *shCsnk1d*-treatment (Extended Data Fig.6f),
195 overexpression of a *shRNA*-resistant CK1δ variant (GFP-CK1$\delta_{RES}$) was used to distinguish
196 the effects of CK1δ KD on the formation of GVBs from its toxic effects (Extended Data Fig.6g-
197 j). Although not sufficient to rescue the toxic effect of CK1δ KD (Extended Data Fig.6k),
198 overexpression of GFP-CK1$\delta_{RES}$ rescued the inhibition of GVB accumulation induced by
199 *shCsnk1d* (Extended Data Fig.6l), further supporting an essential role for CK1δ in the
200 formation of GVBs.
201
202 Next, we investigated if regulation of CK1δ levels or activity underlies its role in GVB formation.
203 Tau aggregation did not alter the total protein level of CK1δ (Extended Data Fig.7a, b) with no

204 difference in somatic CK1δ intensity between GVB- and GVB+ neurons (Extended Data
205 Fig.7c). In contrast, treatment with CK1$\delta_i$ strongly increased CK1δ levels, independent of the
206 presence of tau (Extended Data Fig.7a, b). Moreover, CK1$\delta_i$ increased nuclear CK1δ levels
207 (Fig.3d, e and Extended Data Fig.4p), in line with a previous study that showed localisation of
208 inactive CK1δ to the nucleus[28]. To exclude that the effect of CK1$\delta_i$ on GVBs was indirectly
209 caused by a changed balance in cytosolic-to-nuclear CK1δ levels, we employed GFP-CK1δ
210 with a nuclear export signal (GFP-CK1δ-NES) to force its cytosolic localization (Fig.3f). GFP-
211 CK1δ-NES selectively localized to GVBs (Extended Data Fig.7d, e), indicating that the NES
212 sequence does not interfere with the localization of CK1δ to GVBs. Upon treatment with CK1$\delta_i$,
213 GFP-CK1δ relocalised to the nucleus like endogenous CK1δ, whereas -as expected- the
214 localisation of GFP-CK1δ-NES was not changed (Fig.3g, h). However, GFP-CK1δ-NES was
215 not able to rescue the CK1$\delta_i$-induced decrease in number of GVB+ neurons (Fig.3i), indicating
216 that the activity of CK1δ directly affects the formation of GVBs. To further support the direct
217 involvement of CK1δ activity in GVB formation, GFP or GFP-CK1δ[14] was overexpressed in
218 tau+ neurons (Fig.3g). GFP-CK1δ+ neurons were 1.72 times more likely to form GVBs than
219 GFP+ neurons (Fig.3j). Moreover, the effect of GFP-CK1δ overexpression on GVBs was lost
220 when neurons were treated with CK1$\delta_i$ (Fig.3j). This demonstrated that the activity of CK1δ is
221 required to generate GVB+ neurons.
222
223 To study the connection between CK1δ and autophagy in GVB formation, we assessed
224 whether increased CK1δ activity can circumvent autophagy inhibition. To this end, we
225 employed a doxycyclin (Dox)-inducible expression system for GFP-CK1δ (Dox-GFP-CK1δ,
226 Extended Data Fig.7f, g). Increasing CK1δ levels by the addition of Dox before inhibition of
227 autophagy with Sar405 rescued GVB formation (Fig.3k, l). To assess if in turn increased
228 autophagy can also compensate for decreased CK1δ activity, autophagy was stimulated with
229 Torin1, before treatment with CK1$\delta_i$ (Fig.3m). Torin1 did not rescue the CK1$\delta_i$-induced
230 reduction in GVB+ neurons (Fig.3n). These results suggest that CK1δ can override impaired
231 autophagic flux and place CK1δ activity upstream in the pathway leading to GVBs.
232

233 **CK1δ accumulation in GVBs marks the appearance of GVB+ neurons**

234 To better understand the connection between the role of CK1δ activity in GVB formation and
235 its accumulation inside GVBs, we first investigated whether the effect of CK1$\delta_i$ on GVB+
236 neurons is binary (GVB+ or GVB- neuron) or more continuous (affecting the number of GVBs
237 per neuron). To this end, the effect of CK1$\delta_i$ treatment on GVBs was analysed by high-
238 resolution confocal microscopy (Fig.4a). This demonstrated that inhibition of CK1δ decreased
239 the number of GVBs within a single neuron, but not the size or the GVB over cytosol (G/C)

240 ratio of CK1δ fluorescence intensity of individual GVBs (Fig.4b-d). These data indicate that
241 CK1δ activity stimulates the formation of GVBs also after the first GVBs have formed.
242
243 To investigate the role of CK1δ activity in CK1δ localization to GVBs more directly, a kinase-
244 dead K38M CK1δ mutant was employed (Extended Data Fig.7e)[28,29]. GFP-CK1δ-K38M
245 selectively accumulates in GVBs (Fig.4e), albeit with a lower G/C ratio (2.5) than wildtype
246 (WT) GFP-CK1δ (3.8; Fig.4f). This indicates that although CK1δ activity is necessary for GVB
247 formation, the activity of an individual CK1δ molecule (*in cis* activity) is not required for its
248 specific accumulation in the core of GVBs.
249
250 To study the dynamics of CK1δ accumulation in GVBs, we used the Dox-inducible expression
251 system for GFP-CK1δ. Dox-GFP-CK1δ was first detected in GVBs 24h after induction and
252 strongly increased at 48h, after which it started to plateau (Fig.4g, h), indicating that a steady-
253 state of newly labelled GVBs is obtained at this point. In the presence of $CK1\delta_i$ (condition 1-
254 3, Fig.4g), the formation of neurons with Dox-GFP-CK1δ+ GVBs was completely prevented
255 (Fig.4h). Because CK1δ activity *in cis* is not required for GVB localisation (Fig.4e), this
256 suggests that the targeting of CK1δ to the core of GVBs is directly coupled to the formation of
257 GVBs. To formally exclude the possibility that rather than inhibiting the formation of new GVBs,
258 $CK1\delta_i$ stimulates the turnover of already formed GVBs, Dox-GFP-CK1δ expression was
259 induced 24h or 48h before $CK1\delta_i$ treatment (condition 4-5, Fig.4g). $CK1\delta_i$ treatment reduced
260 the number of Dox-GFP-CK1δ+/GVB+ neurons, but did not completely block it (Fig.4h). This
261 indicates that the remaining Dox-GFP-CK1δ+/GVB+ neurons were formed before $CK1\delta_i$ was
262 added. Consequently, we were able to calculate the stability of GVBs. Since CK1δi blocks
263 new GVB formation, the observed GVB+ neurons (Extended Data Fig.4o) existed before
264 treatment. The difference between expected (Fig.1h) and observed GVB+ neurons (Extended
265 Data Fig.4o) was used to calculate an average $t_{1/2}$ of 5.4 days (Extended Data Fig.8a). This
266 is supported by live cell microscopy of GFP-CK1δ-labeled GVBs, demonstrating that GVBs
267 were relatively stable for at least 9h (Supplementary Video1), indicating a low-turnover rate.
268 Furthermore, using fluorescence recovery after photobleaching (FRAP) imaging, we observed
269 that no new CK1δ is incorporated into the pre-existing GVBs over a span of ±17h (Fig.4i).
270 These collective data identify CK1δ as an upstream regulator of GVB formation and indicate
271 that CK1δ is targeted to the GVB core during this process. Given the stability of the CK1δ
272 accumulations in GVBs, they reflect the initiation of the GVB condition in the neuron.
273

274 **GVB+ neurons are resilient to tau-induced protein synthesis impairment**

275 To investigate potential functional implications of the presence of GVBs, early proteome
276 changes induced by tau pathology at day 15 were determined (Fig.5a and Supplementary
277 Table 1). Gene ontology (GO) analysis indicated that the upregulated functional processes
278 primarily involved pathways affecting the synapse (Fig.5b) in line with the tau/GVB model
279 representing an early stage preceding neurodegeneration (Extended Data Fig.1a-o). The most
280 significantly downregulated functional protein groups are solute carrier membrane transport
281 proteins, predominantly amino acid transporters (Fig.5b). This may impact the availability of
282 amino acids for the biosynthesis of proteins and may point to reduced protein synthesis as an
283 early tau-induced process. To directly determine *de novo* protein synthesis in relation to tau
284 pathology and GVB condition, we employed the SUnSET puromycin labelling assay[30,31]
285 combined with quantitative high-content automated microscopy to analyse tau- and tau+
286 neurons at day 22. We developed a script to differentiate between tau+/GVB- and tau+/GVB+
287 neurons within the tau+ population. Tau+/GVB- neurons, which constitute the majority of tau+
288 neurons, displayed a pronounced reduction in protein synthesis rates of 31% compared to
289 tau- neurons (Fig.5c, d). In contrast, tau+/GVB+ neurons retained protein synthesis rates
290 similar to those of tau- neurons (Fig.5c, d).
291
292 To study the mechanism underlying these differences, we investigated the involvement of
293 transient adaptation of protein synthesis rates by proteostatic stress responses, where the
294 integrated stress response (ISR) is a central player (Fig.5e). To test whether the ISR is
295 activated, the nuclear intensity of the ISR target ATF4 upon tau aggregation was assessed.
296 This demonstrated a small increase in ATF4 levels in the GVB+ population, making it unlikely
297 that the ISR activation underlies the tau-induced protein synthesis decline, as would have
298 resulted in a higher signal in the GVB- neurons (Fig.5f). However, because ATF4 induces the
299 expression of factors involved in amino acid metabolism[32], we assessed the levels of SLC3A2,
300 a component of the major neutral amino acid transporter that was downregulated by tau
301 aggregation (Fig.5a). SLC3A2 levels were found to be 22% higher in tau+/GVB+ neurons
302 compared to tau+/GVB- neurons (Fig.5g), potentially contributing to increased free amino
303 acids for protein synthesis in GVB+ neurons. To test if the GVB+ neurons actively maintained
304 protein synthesis rates or were less responsive to ISR-induced protein synthesis reduction,
305 neurons were treated with the ISR inducer tunicamycin (TM). TM treatment resulted in a strong
306 reduction in protein synthesis and increased nuclear ATF4 intensity independent of the
307 presence of tau pathology or GVBs (Fig.5h, i and Extended Data Fig.9a). This shows that
308 GVB+ neurons can dynamically adjust their protein synthesis levels in response to stress,
309 indicating that they exhibit resilience to tau-induced impairment in *de novo* protein synthesis.

310 Moreover, 48h TM treatment did not alter the number of GVB+ neurons (Extended Data
311 Fig.9b). Furthermore, inhibition of the activity of the different ISR kinases (EIF2AK1-4: HRI,
312 PKR, PERK, GCN2, respectively; Fig.5e) using a pharmacological inhibitor of EIF2AK3
313 ($PERK_i$) or knock-down of *Eif2ak1, 2 or 4* (validated previously[31]) did not alter the formation of
314 GVB+ neurons (Extended Data Fig.9c, d), further supporting that the ISR is not involved.
315 Protein synthesis can also be transiently reduced by the mTOR pathway. However, there was
316 no difference in the phosphorylation of the mTOR substrate 4E-BP1 neurons without and with
317 tau pathology, suggesting that the mTOR pathway is not activated in the pool of tau+ neurons
318 (Extended Data Fig.9e, f). Also, treatment with pharmacological inhibitors of the mTOR- and
319 Angiogenin-mediated stress pathways did not affect protein synthesis rates in tau+/GVB- or
320 tau+/GVB+ neurons (Extended Data Fig.9g, h). These collective data show that transient
321 stress pathways are not directly involved in the tau-induced protein synthesis reduction or the
322 resilience there to in GVB+ neurons.
323
324 To determine whether adaptations in the protein synthesis machinery itself underlie the
325 resilience, we measured the levels of ribosomal proteins and biogenesis factors in tau+
326 neurons. The levels of ribosomal proteins RPL24, RPL15 and RPS12 were increased in
327 tau+/GVB+ neurons compared to tau+/GVB- neurons by 16%, 9% and 18%, respectively
328 (Fig.5j-l). Also the levels of ribosomal assembly factors BYSL and LTV were 20% higher in
329 tau+/GVB+ neurons (Fig.5m, n). To investigate whether the GVB itself functions as a localized
330 hub for protein synthesis, we assessed the colocalization of GVBs with key components of the
331 translation machinery using confocal microscopy. We stained for RNA, using RNASyto Green,
332 nascent proteins via puromycin pulse labelling and RPS12 and RPL24 (Fig.5o-r). No overlap
333 was observed between these markers and GVBs, making it unlikely that GVBs themselves
334 directly contribute to protein synthesis. These results suggest that GVB+ neurons have elicited
335 a response to ameliorate reduced protein synthesis upon tau aggregation that includes
336 increased ribosomal content.
337

338 **GVB+ neurons fully retain the capacity to control LTP-regulated protein synthesis in**
339 **the presence of tau pathology**

340 We showed that GVB+ neurons are resilient to tau-induced neurodegeneration (Fig.1e-g). To
341 investigate whether the increased survival of GVB+ neurons is related to protein synthesis
342 capacity, protein synthesis was inhibited using 48h of anisomycin treatment (Fig.6a), which
343 reduced protein synthesis to a similar extent in GVB- and GVB+ neurons, 66% and 65%
344 respectively (Fig.6b). However, while anisomycin treatment resulted in a 28% reduction to
345 control in the number of GVB- neurons, GVB+ neuron number was unaffected (Fig.6c). These

346 results suggest that GVB+ neurons are more resilient to toxicity induced by protein synthesis
347 inhibition.
348
349 To study the relevance of the resilience of GVB+ neurons for neuronal function, we assessed
350 the capacity of tau+ neurons to regulate the acute synthesis of immediate early genes (IEGs)
351 that are involved in the changes of synaptic strength, which is essential for learning and
352 memory-related processes[33,34]. To study if tau aggregation also reduces long-term
353 potentiation (LTP)-related IEG induction in our model, neuronal plasticity was induced using
354 4BF for 4h after 15 days of tau exposure. 4BF induces chemical LTP and induces the
355 expression of the IEGs ARC and c-FOS[35]. Quantitative high-content automated microscopy
356 was employed to determine expression levels of ARC and c-FOS in the nucleus of tau-,
357 tau+/GVB- and tau+/GVB+ neurons. Both ARC and c-FOS expression were strongly
358 increased upon the induction of chemical LTP (Fig.6d-g). In tau+/GVB- neurons, ARC and c-
359 FOS levels upon LTP induction were significantly lower than in tau- neurons (decreased by
360 34% and 19%, respectively), while the tau+/GVB+ neurons do not differ or are even higher in
361 ARC and c-FOS expression levels from tau- neurons, respectively (Fig.6f, g). As expected,
362 the upregulation of ARC and c-FOS upon LTP induction was dependent on *de novo* protein
363 synthesis as anisomycin reduced the increase of these proteins (Fig.6f, g and Extended Data
364 Fig.10 a, b). These data show that GVB+ neurons are resilient to tau-induced impairment in
365 LTP-regulated protein synthesis.

366 **Discussion**

367 In response to pathological protein assemblies, including tau and α-synuclein, neurons can
368 develop GVBs[14,15]. In the human AD brain -like in our model- GVB+ neurons are the surviving
369 neurons upon neuronal loss with increased disease severity[12,36,37], in accordance with a
370 protective rather than a degenerative role. Our collective data support a model where GVB+
371 neurons have adapted to tau-induced reduction of protein synthesis (see model in Fig.7). Our
372 findings demonstrate that CK1δ activity is essential for GVB formation. In addition, we show
373 that autophagy but not endocytosis is required for GVB formation. Activation of autophagy
374 does not affect the number of GVB+ neurons and does not rescue GVB formation when CK1δ
375 is inhibited. In contrast, overexpression of CK1δ enhances the GVB+ neuron number and
376 overrides inhibition of autophagy, identifying it as a rate-limiting factor. Our data are compatible
377 with a CK1δ-driven process that employs the basal autophagic machinery.
378
379 Disturbed translational regulation and overall protein synthesis impairment are observed in
380 models of tauopathies[2–6] and several other neurodegenerative proteinopathies[38–43]. Therefore,
381 impaired protein synthesis is considered an important pathogenic mechanism in
382 neurodegenerative diseases, supported by the amelioration of neurodegenerative phenotypes
383 by the rescue of protein synthesis[5,43–46]. Prolonged reduction of protein synthesis rates affects
384 neuronal viability and function by impairing replacement of critical structural proteins, but also
385 by directly affecting synaptic plasticity, which requires adequately regulated *de novo* protein
386 synthesis[47,48]. The acute and dynamic demand for protein synthesis that is required for
387 synaptic plasticity includes the rapid induction of IEG proteins. Tau pathology has been
388 demonstrated to impair synaptic plasticity, as well as the expression of IEGs in animal
389 models[49,50]. Also in our model, tau aggregation reduces global protein synthesis rates as well
390 as the LTP-regulated induction of IEGs c-FOS and ARC. c-FOS is synthesized in response to
391 increased neuronal activity[51,52] and ARC is required for the consolidation of LTP and
392 maintenance of synaptic strength[53,54], both essential for learning and memory-related
393 processes[33,34]. Our data demonstrate that GVB+ neurons not only retain global protein
394 synthesis rates similar to those of neurons without tau pathology, but also importantly retain
395 the capacity to adequately regulate LTP-related IEG protein expression. This demonstrates
396 that GVB+ neurons are resilient to tau pathology-induced protein synthesis decline.
397
398 To identify the mechanism by which GVB+ neurons adapt to the tau-induced protein synthesis
399 decrease, transient proteostatic responses mediated by the ISR, mTOR and Angiogenin were
400 investigated. No evidence for their involvement in GVB+ neurons was found, suggesting that
401 the rescue of protein synthesis involves an adaptation of the protein synthesis machinery.

402 Paradoxically, a small increase in nuclear levels of the ISR-induced transcription factor ATF4
403 was found in GVB+ neurons. Although this excludes the involvement of the ISR in the global
404 protein synthesis rescue in GVB+ neurons, it may explain the expression of ATF4-regulated
405 factors like the amino acid transporter SLC3A2[32], which is increased in GVB+ neurons. In AD,
406 progressive ribosomal loss correlates with tau pathology[55], aligning with studies in tauopathy
407 mouse models that demonstrate decreased ribosomal protein synthesis accompanied by
408 reduced overall protein synthesis[6]. Moreover, targeted laser capture proteomics of human AD
409 hippocampus demonstrated that tangle-bearing neurons exhibit a loss of ribosomal proteins;
410 however, in GVB+ neurons the ribosomal protein levels are similar to those in neurons without
411 tau pathology[56]. We demonstrate here that GVB+ neurons have increased levels of the small
412 ribosomal subunit protein RPS12, the large ribosomal subunit proteins RPL15 and RPL24 as
413 well as the ribosomal biogenesis factors LTV1 and BLTV.
414
415 Interestingly, while GVB+ neurons exhibit an autolysosomal response accompanied by
416 increased lysosomal content, this does not significantly contribute to the degradation of
417 pathological tau aggregates, as tau pathology is not different between GVB- and GVB+
418 neurons[15]. Proteomics analysis showed that in a stage preceding neurodegeneration, tau-
419 pathology induces reduced levels of several amino acid transporters. Given the close
420 collaboration between autolysosomal degradation and amino acid transporters in the
421 maintenance of the free amino acid pool[57], we propose that the increased lysosomal content
422 functions to generate amino acids to boost protein synthesis in GVB+ neurons. Whereas
423 classical proteostatic stress responses involve increased lysosomal capacity and reduced
424 protein synthesis, GVB+ neurons have initiated a unique proteostatic program that increases
425 both lysosomal and ribosomal content. This shows that GVB+ neurons have multiple
426 adaptations that allow them to counteract the tau pathology-induced decline in protein
427 synthesis (Fig.7), supported by the resilience of GVB+ neurons to protein synthesis inhibition.
428
429 GVBs have similar degradative capacity as the non-GVB lysosomes in the same cell and are
430 distinguished by the presence of one or multiple dense cores[14]. Live-cell imaging and half-life
431 calculations show that GVB cores are highly stable. Inhibition of autophagy does not result in
432 accumulation of GVB cores in the cytosol, indicating that they either form within
433 autolysosomes or originate in the cytosol but are rapidly degraded if not engulfed. The
434 prominent presence of CK1δ in the core could indicate a negative feedback mechanism to
435 sequester the key regulator of the protective mechanism in GVB+ neurons to prevent
436 overactivation of the pathway. Although CK1δ activity is required for the resilience of GVB+
437 neurons, CK1δ activity *in cis* is not required for its localization to GVBs. The collective data
438 are in agreement with a model where the accumulation of CK1δ in GVBs occurs during the

formation of GVB+ neurons. The lack of interventions that can disconnect the resilience program in GVB+ neurons and the formation of GVBs makes it difficult to conclusively assess whether GVBs are merely a byproduct of activation of the protective mechanism in GVB+ neurons. However, currently, there is no indication for a specific function associated with GVBs themselves.

Follow-up studies should address how tau aggregates induce CK1δ activity and what substrates are involved in resilience. CK1δ is traditionally considered a constitutively active protein, relying on binding partners or scaffold proteins for subcellular localization[58,59], although differential autophosphorylation was more recently shown to regulate substrate selectivity[60]. CK1δ binds to and phosphorylates tau at different sites[59]. Tau assemblies may provide a platform for CK1δ binding and signalling, leading to GVB formation. This may involve structural rather than primary sequence motifs because GVBs also form in response to α-synuclein aggregates[15], although the involvement of CK1δ and protein synthesis resilience in α-synuclein-induced GVBs has currently not been demonstrated. The number of neurons with tau pathology that become GVB+ increases over time, suggesting a (partially) stochastic process. The high toxicity of CK1δ KD and the strongly increased levels of CK1δ upon inhibition of its activity suggest that neurons require tight regulation of CK1δ that may also involve a non-catalytic role of the protein. CK1δ has been implicated in autophagy[61–64] and was previously demonstrated as a critical regulator of ribosome assembly through phosphorylation of assembly factors LTV1 and BYSL[65,66]. The increased levels of these factors in GVB+ neurons, together with increased levels of ribosomal proteins, support a mechanism involving ribosomal biogenesis.

The identification of specific molecular targets to stimulate GVB formation has therapeutic potential. Because GVBs form selectively in neurons, it is likely that, in addition to CK1δ, cell type-specific factors are involved. Ultimately, combining resilience-boosting therapy with tau-reducing therapies like *MAPT* antisense oligonucleotides or tau immunotherapy is an attractive scenario to halt the disease while also protecting neurons against the cellular effects of tau pathology to help them to retain function. By elucidating the mechanistic underpinnings of the formation and functional implications of the presence of GVBs in neurons, our work offers new insights into neuronal resilience in tauopathies.

**Acknowledgements**

We thank Bart Klein for expert technical support, Joke Wortel for animal breeding and Robbert Zalm and Ingrid Saarloos for plasmid construction and lentivirus production. We also would

like to thank the Molecular Neurodegeneration group and our Functional Genomics Department colleagues for stimulating discussions and critical reading of the manuscript. This work was supported by Hersenstichting/Coby van Nieuwkerkfonds #DR-2019-00278, Alzheimer Nederland #WE.03-2017-10 and The Netherlands Organisation for Scientific Research (NWO) #OCENW.M.21.123 to WS.

480 **Methods**

481 **Animals and primary cell culture**

482 Animals were kept and bred according to institutional and Dutch governmental guidelines and
483 experiments were approved by the animal ethical committee of the VU University/VU
484 University Medical Center. C57BL/6 mice were bred in-house or obtained from Charles River.
485
486 Embryonic day (E) 18.5 WT mouse embryos or postnatal day 1 (P1) mice were dissected to
487 obtain cerebral cortices after disposal of the meninges. The cortices were digested in Hanks
488 balanced salt solution (HBSS, Sigma-Aldrich) containing 10 mM HEPES (Gibco; Hanks-
489 HEPES) and 0.25% trypsin (Gibco) for 20 min at 37°C. Hereafter, the digested tissue was
490 washed twice with Hanks-HEPES and subsequently with DMEM (Lonza) containing 10% heat-
491 inactivated fetal bovine serum (Gibco), 1% penicillin-streptomycin (Gibco) and 1% non-
492 essential amino acid solution (Gibco; DMEM+) in which the tissue was triturated using a fire-
493 polished Pasteur pipette. Subsequently, the dissociated cells were spun down for 5 min at
494 800g at room temperature (RT), resuspended and plated in neurobasal medium (Gibco)
495 supplemented with 2% B-27 (Gibco), 18 mM HEPES, 0.25% Glutamax (Gibco) and 0.1%
496 penicillin-streptomycin (NB+).
497
498 Primary cortical neurons were cultured in plates and glass coverslips coated with 5 µg/mL
499 poly-L-ornithine (Sigma-Aldrich) and 2.5 µg/mL laminin (Sigma-Aldrich and Bio-Techne)
500 overnight (O/N) at room temperature (RT). All cells were maintained at 37°C and 5% $CO_2$. For
501 Western blotting, cortical neurons were plated in a 6-well plate at a density of 300.000 neurons
502 per well. For immunolabeling, neurons were plated on 13 mm glass coverslips or in a 96-well
503 plate (Greiner) at a density of 40.000 cells or 12.500 cells per well, respectively. After 10 days
504 *in vitro* (DIV10), fresh NB+ was supplied to each well at 40% of the total volume in the well.
505

506 **Lentiviral transduction in primary cells**

507 Lentiviral transduction with the human 2N4R P301L, S320F tau ($FTDtau^{1+2}$) and $FTDtau^{1+2}$
508 with an in-frame C-terminal EGFP tag ($FTDtau^{1+2}$-GFP) were performed on DIV3 (Day0),
509 unless otherwise specified, in primary neurons[15,16,27].
510
511 WT mouse CK1δ (kind gift from Dr. Y.E. Greer) has been described before[67] and the formation
512 of N-terminally tagged CK1δ with EGFP (GFP-CK1δ) has been described before[14]. GFP-
513 $CK1\delta_{RES}$ was changed from WT CK1δ in the *shCsnk1d* target sequence to prevent KD (Table
514 1) (new sequence: CGGGA**C**CG**T**GA**G**GAACGATTA). A nuclear export signal (NES) was N-

515 terminally cloned into the GFP-CK1δ construct. For the kinase-dead variant of CK1δ, a single
516 point-mutation in lysine-38 to methionine-38 (AAG to ATG) was created to form GFP-CK1δ-
517 K38M. As a control for EGFP-tagged constructs, a lentiviral CMV-driven EGFP construct was
518 used. All constructs were subcloned into lentiviral backbone vectors under the
519 cytomegalovirus (CMV), the neuron-specific synapsin (Syn) or a doxycycline-inducible Syn
520 promoter using the Gateway system (Invitrogen). The production of lentiviral particles was
521 performed as described previously[68] and the lentiviral particles were stored at -80°C until use.
522
523 Plasmids for short hairpin RNA (shRNA) constructs for the scrambled control (*shScr*), CK1δ
524 (Sigma-Aldrich; TRCN0000023773) and EIF2AK1/2/4 were obtained from the MISSION
525 shRNA library (Sigma-Aldrich; TRCN0000028788, TRCN0000027041, TRCN0000028842)
526 and previously validated in our lab[31]. shRNAs targeting FIP200 (kind gift of Dr. Marijn
527 Kuijpers)[19] and ATG5 was cloned using oligonucleotides (Sigma-Aldrich) based on previously
528 published research[20]. The shRNAs were cloned into a second-generation lentiviral backbone
529 under a CMV promoter.
530
531 Table 1: The names, targeting gene and sequence of the shRNA of all shRNAs used in this
532 research.

| **Name** | **Gene** | **Sequence** |
|---|---|---|
| *shScr* | - | CCGCAGGTATGCACGCGT<br>or<br>TTCTCCGAACGTGTCACGT |
| *shCsnk1d* | CK1δ | CGGGATCGAGAAGAACGATTA |
| *shFip200* | FIP200 | GAGAGAACTTGTTGAGAAA |
| *shAtg5* | ATG5 | GCAGAACCATACTATTTGCTT |
| *shHri* | EIF2AK1 | GCTCGGAATTGGAAGGGAATT |
| *shPkr* | EIF2AK2 | CGCCAGGTTTAACAGCGATTT |
| *shGcn2* | EIF2AK4 | GCCAACCATCAACTCACTAAT |

533
534 All lentiviral constructs were transduced on DIV10 (day 7), except FTDtau$^{1+2}$(-GFP) (specified
535 in the text), *shCsnk1d-1* and the *shScr* as control on DIV14 (day 11) and GFP-CK1$\delta_{RES}$ and
536 GFP as control on DIV7 (day 4).
537

538 **Cell treatments**

539 Primary neurons were treated with 50 µM E64D and 20 µM Pepstatin-A (Sigma-Aldrich) for
540 24h. For the inhibition of endocytosis, neurons were sequentially incubated on DIV16 (day 13)
541 and DIV17 (day 14) with 10 uM Dyngo4a (final concentration is 20 uM; Bio-Connect) and 0.5
542 µg/ml Filipin3 (final concentration is: 1.0 ug/ml; Sigma-Aldrich). 5 µM of Sar405 (Sigma-
543 Aldrich) was used for indicated times to inhibit VPS34 and 5 µM Torin1 (Bioke) (72h, 48h or
544 24h) or 1 µM rapamycin (Hello Bio) (48h) were used to inhibit mTOR. To inhibit CK1δ, neurons
545 were treated with PF-670462 ($CK1\delta_i$, TargetMol) for indicated times at a concentration of 12.5
546 µM. To induce ER-stress, primary neurons were treated with tunicamycin (TM, Sigma-Aldrich)
547 for 24h or 48h at 5 µg/ml. PERK inhibitor (GSK2606414, Sigma-Aldrich) was added 48h before
548 fixation at a final concentration of 0.5 µM. Angiogenin inhibitor (NSC-65828, National Cancer
549 Institute) was added 24h before fixation at a final concentration of 75 mM. PERK inhibitor and
550 angiogenin inhibitor were previously validated[31]. Anisomycin (Sigma-Aldrich) was added for
551 48h, or directly before the induction of LTP, at a final concentration of 50 ng/ml to determine
552 the effect on global protein synthesis. To label *de novo* synthesised proteins, we performed
553 surface sensing of translation (SUnSET) as previously described[30]. In short, primary cells were
554 incubated with 2 µM puromycin (InvivoGen) for 15 min before fixation. Using the anti-
555 puromycin antibody (see Supplementary Table 1), puromycinylated proteins were detected.
556 To stain nucleic acids, cells were incubated with 1 µM SYTO RNASelect (Thermo Fisher
557 Scientific) for 4 hr before methanol fixation. Compounds were dissolved in $H_2O$ (puromycin)
558 or DMSO (the rest) and diluted in NB+. Equal amounts of solvent were added to the control
559 conditions or when multiple concentrations were used, the highest concentration was used to
560 determine the amount of vehicle added.
561

562 **Induction of chemical LTP**

563 Neurons at DIV18 (day 15) were stimulated for 4 hours, after which they were directly fixed. A
564 cocktail of chemicals was used to induce network activity and plasticity for generation of
565 immediate early gene (IEG) expression. The 4BF cocktail consists of 100 µM 4-aminopyridine
566 (Sigma, A78403), 50 µM bicuculline (Sigma, 14343) and 50 µM forskolin (Sigma, 344282) as
567 previously described[35].
568

569 **Fixation and immunolabeling of primary neurons**

570 On DIV18 (day 15), DIV25 (day 22) or DIV32 (day 29) neurons were fixed in 1.85%
571 formaldehyde (FA, Electron Microscopy Sciences) in PBS (pH 7.4) by the addition of equal
572 volumes of 3.7% FA to the culture medium for 10 min followed by fixation in 3.7% FA for 10

573 min at RT. Primary neurons shown in Fig.5r and Extended Data Fig.5 v were fixed in ice-cold
574 methanol for 15 min on ice to remove soluble proteins. After fixation, cells were washed with
575 PBS and stored at 4°C in PBS (pH 7.4) in the dark until further use. Fixed cells were
576 permeabilised in 0.5% Triton X-100 (Thermo Fisher Scientific) in PBS (pH 7.4) for 5 min at RT
577 and blocked in 2% normal goat serum (Gibco) and 0.1% Triton X-100 in PBS (blocking
578 solution) for 30 min at RT. Primary antibodies were diluted in blocking solution and incubated
579 O/N at 4°C in the dark. The primary antibodies used and their dilutions are listed in Table 2.
580 After 3 PBS washes, cells were incubated with Alexa Fluor (405, 488, 546, 568, 647)-
581 conjugated secondary antibodies (Abcam and Thermo Fisher Scientific) in a 1:500 dilution in
582 blocking solution for 1 h at RT in the dark. Cells were subsequently washed thrice with PBS.
583 Aggresomes were visualised using the proteostat aggresome detection kit (Enzo) according
584 to the manufacturer's details and washed three times with PBS. Hereafter, to visualise nuclei,
585 cells were incubated with DAPI (Brunschwig Chemie) diluted in PBS (5 µg/mL) at RT for 5
586 min, followed by two PBS washes. Coverslips were mounted on microscope slides (Thermo
587 Fisher Scientific) using Mowiol (Sigma-Aldrich) and were kept in the dark O/N at RT to dry.
588 Slides were stored in the dark at 4°C until imaging. 96-well plates were stored in the dark at
589 4°C until imaging with the wells filled with 100 µl PBS.
590
591 Table 2: Antibodies used in this research. From left to right: The target protein the primary
592 antibody was raised at; for antibodies targeting specific phosphor-sites, the phospho-epitope
593 is listed; the species of the primary antibody; the dilution used for immunofluorescence (IF) or
594 western blot (WB); the source; the product number.

| **Antibody** | **Phospho-epitope** | **Species** | **Dilution** | | **Source** | **Product number** |
|---|---|---|---|---|---|---|
| | | | **IF** | **WB** | | |
| AT8 | Ser202/Thr205 | Mouse monoclonal | 1:400 | | ThermoScientific | MN1020 |
| ATG5 | | Rabbit polyclonal | | 1:1000 | Proteintech | 10181-2-AP |
| ARC | | Rabbit polyclonal | 1:500 | | Synaptic Systems | 156 003 |
| BYSL | | Rabbit polyclonal | 1:250 | | ThermoScientific | PA5-56679 |
| c-FOS | | Rat monoclonal | 1:1000 | | Synaptic Systems | 226 017 |
| CK1δ | | Mouse monoclonal | 1:1000 | 1:2000 | Santa Cruz Biotechnology | sc-55553 |

| | | | | | | |
|---|---|---|---|---|---|---|
| FIP200 | | Rabbit monoclonal | | 1:1000 | Cell signaling | 12436S |
| GOLGA4 | | Rabbit polyclonal | 1:2000 | | Sigma-Aldrich | HPA0351021 |
| GFP | | Rabbit polyclonal | | 1:500 | Bio-Connect | GTX20290 |
| LAMP1 | | Rat monoclonal | 1:500 | | BioLegend | 121601 |
| LAMP1 | | Rat monoclonal | 1:1000 | | Abcam | ab25245 |
| LIMP2 | | Rabbit polyclonal | 1:500 | | Novus Biologicals | NB400-129 |
| LTV1 | | Rabbit polyclonal | 1:250 | | ThermoScientific | PA5-56373 |
| MAP2 | | Chicken polyclonal | 1:500 | | Abcam | ab5392 |
| MC1 | | Mouse monoclonal | 1:500 | | Kind gift from Dr. Peter Davies | |
| pPERK | Thr981 | Rabbit polyclonal | 1:1000 | | Santa Cruz Biotechnology | sc-32577 |
| pPERK | Thr982 | Rabbit polyclonal | 1:500 - 1:1000 | | ThermoScientific | PA5-102853 |
| Puromycin | | Mouse monoclonal | 1:500 | | Milipore | MABE343 |
| Puromcyin | | Mouse monoclonal | 1:3000 | | Kerafast | EQ0001 |
| P62 | | Rabbit polyclonal | | 1:2000 | ThermoScientific | PA5-20839 |
| RPL15 | | Rabbit polyclonal | 1:250 | | Proteintech | 16740-1-AP |
| RPL24 | | Rabbit polyclonal | 1:250 | | Proteintech | 17082-1-AP |
| RPS12 | | Rabbit polyclonal | 1:250 | | Proteintech | 16490-1-AP |
| SLC3A2 | | Rabbit polyclonal | 1:400 | | Proteintech | 15193-1-AP |

| | | | | | | |
|---|---|---|---|---|---|---|
| SYP1 | | Guinea pig polyclonal | 1:1000 | | Synaptic Systems | 101004 |
| 4E-BP1 | | Rabbit monoclonal | | 1:1000 | Cell Signaling Technology | 9644 |
| p-4E-BP1 | Thr37/Thr46 | Rabbit monoclonal | | 1:1000 | Cell Signaling Technology | 2855 |

595

596 **Confocal microscopy and confocal image analysis**

597 The mounted coverslips were imaged using a Nikon Eclipse Ti confocal microscope controlled
598 by NisElements 4.30 software (Nikon), equipped with a 60x oil immersion objective (NA = 1.4)
599 or a 40x oil immersion objective (NA = 1.3). Z-stacks with a step size of 0.25, 0.5 or 1 µm were
600 obtained. Laser settings were adjusted to reduce saturation and kept the same in every
601 independent experiment between conditions.
602

603 **Live microscopy**

604 The cells were placed in a Tokai Hit live-cell microscope incubation system mounted in the
605 Nikon Eclipse Ti confocal microscope, equipped with a 40x oil immersion objective (NA = 1.3)
606 or a 10x air objective (NA = 0.45) for calcium imaging. 10 min before calcium imaging, 0.5 µM
607 X-Rhod-1 (Thermo Fisher Scientific) was added to the cells. A video with 8fps was made for
608 the duration of 5 min. For following GVB dynamics, every 10, 20 or 30 min for a period of
609 minimally 9h, a Z-stack with a step size of 1 µm was obtained. When FRAP was applied, a
610 specified region in the GVB+ soma was photobleached and followed over the same period as
611 described in the text.
612

613 Confocal images were analysed using ImageJ software (National Institutes of Health).
614 Neurons with 2 or more CK1δ or pPERK bright punctae were defined as GVB+ neurons and
615 neurons without any punctae were defined as GVB- neurons. Single confocal planes are
616 shown unless otherwise stated.
617

618 Line segments were drawn to determine the overlap between multiple markers. The line
619 graphs show fluorescence intensity in arbitrary units (AU).
620

621 The amount and size of somatic lysosomes were determined using an in-house developed
622 script named "LysoFinder", which is publicly available (https://git.vu.nl/public-neurosciences-
623 fga/imagej-apps/lysofinder). The amount, intensity and size of GVBs in neurons transduced

624 with the GFP, GFP-CK1δ and GFP-CK1δ-K38M constructs or neurons treated with $CK1\delta_i$
625 were determined using an adapted version of the LysoFinder script. In short, maximum
626 intensity projections were created and based on a pPERK mask, the amount and size of single
627 GVBs within a manually drawn neuronal soma were determined. The intensity of the protein
628 of interest was measured within the GVB-mask and outside the mask within the soma. The
629 ratio of the intensity in the GVB over cytosol (G/C) was then calculated and was used to
630 determine the GVB-selective localization of the protein.
631

632 **High-throughput microscopy and automated analysis**

633 Cells cultured in a 96-well plate were imaged using CellInsight CX7 High-Content Screening
634 (HCS) Platform (Thermo Fisher Scientific) controlled by HCS Studio Cell Analysis software
635 (Thermo Fisher Scientific). 10x, 20x and 40x air objectives were used in widefield mode. The
636 10x or 20x objectives were used to determine toxicity of the treatment compared to control.
637 The 20x objective was used for determination of morphology. The 20x and 40x objectives
638 were used to measure intensity and determine the number of GVB+ neurons. A single focal
639 plane was obtained for all channels. 25 or 30 fields, distributed throughout the well, were
640 imaged for 10x or 20x and 40x, respectively. In all cases, DAPI signal was used for autofocus
641 for every image individually. On average, 10x imaging obtained data from 1000-10000
642 neurons per well, 20x imaging from 50-1000 neurons per well and 40x 25-500 neurons per
643 well.
644

645 The data obtained from the high-throughput microscopy were analysed with Columbus
646 analysis software (v2.5.2.124862; PerkinElmer) by in-house developed scripts. Each script
647 was optimized per independent experiment. In every analysis, neuronal nuclei were defined
648 by overlap between the nuclear marker DAPI and the neuron-specific marker MAP2 as well
649 as the size and roundness of the nucleus. Outcome parameters were averaged per well (when
650 applicable) and normalised to the mean of the control wells. These values were used in the
651 analysis.
652

653 **Neuronal morphology**

654 Dendritic morphology and pre-synaptic density were determined using in-house developed
655 scripts, previously published[27,31]. In short, based on MAP2 staining, dendritic morphology was
656 determined using a built-in CSIRO neurite analysis module. Morphological features, including
657 dendrite length, number of extremities, segments and primary dendrites were normalised to
658 the number of neuronal nuclei within that well. The amount of synaptophysin 1 (SYP1) positive
659 pre-synapses was determined based on local intensity maxima within an enlarged MAP2

660 mask. The pre-synapse density was determined by dividing the total amount or SYP1 puncta
661 over total dendrite length.
662
663 **Tau intensity in MAP2 mask**
664 The intensity measurements of multiple readouts of tau aggregation, GFP-tagged and
665 untagged FTDTau$^{1+2}$, were performed by measuring the sum of the intensity of FTDTau$^{1+2}$-
666 GFP or the conformational pathogenic tau marker MC1 in a MAP2 mask. The absolute
667 intensity was normalised to the total area of the MAP2 mask.
668
669 **GVB selection**
670 GVB+ neurons were defined using an altered protocol, as previously described[14,15]. In short,
671 the GVB marker (pPERK, CK1δ, Dox-GFP-CK1δ or GolginA4) was subjected to a filter step
672 to decrease background intensity using a curvature optimized per marker. Single puncta were
673 selected based on intensity. The single puncta were subsequently clustered based on their
674 proximity to one another. These clusters were defined as GVB-clusters based on their size,
675 roundness, intensity of the GVB-marker, the intensity of MAP2 in the cluster and exclusion of
676 the cluster within the nucleus based on DAPI-signal. The percentage of GVB-clusters was
677 calculated by dividing the number of GVB-clusters by the number of neurons in the same well.
678
679 **Somatic and nuclear intensity**
680 The soma was defined as the MAP2-positive signal 13µm around the neuronal nucleus
681 (excluding overlap between bordering somas), after smoothing and filling the holes of the
682 MAP2 signal. Subsequently, somas in neurons transduced with FTDtau$^{1+2}$ were defined as
683 GVB- or GVB+ as previously described. False positives were excluded in tau- neurons. Within
684 each soma, the mean intensity of the marker (e.g. puromycin, SLC3A2, RPS12, RPL15,
685 RPL24, LTV1 and BYSL) was measured in the complete soma (cytosol and nucleus). Somatic
686 CK1δ levels were determined by measuring CK1δ intensity in the soma without the GVBs.
687 Nuclear intensity for CK1δ was corrected by subtracting the mean nuclear intensity by the
688 mean intensity level of the cytosol without the nucleus. When determining CK1δ levels in a
689 GVB+ neuron, pPERK was used to define GVB-positivity. The nuclear intensity of c-FOS and
690 ARC were not background corrected. The number of GVB+ somas was divided by the number
691 of somas to calculate the percentage of GVB+ somas.
692
693 **GVB selection in GFP-positive neurons**
694 For the selection of GFP-positive (GFP+) neurons, the soma was defined as previously
695 described. Mean GFP intensity was measured in the complete soma region, including the
696 nucleus. Based on an untransduced negative control, a threshold was set to select neurons

697 with a higher somatic mean GFP-intensity than the negative control. These neurons were
698 defined as GFP+ neurons. GVB-clusters were defined as GFP+ if they were localised within
699 the GFP+ soma, creating GVB-/GFP+ and GVB+/GFP+ somas. Within these two populations,
700 mean GFP-intensity was measured in the complete soma (cytosol and nucleus), only the
701 nucleus and the cytosol without the nucleus. Nuclear intensity was corrected by subtracting
702 the mean nuclear intensity by the mean intensity level of the cytosol excluding the nucleus
703 and GVBs, per neuron. The number of GVB+/GFP+ neurons was divided by the number of
704 GFP+ neurons to calculate the percentage of GVB+/GFP+ neurons.
705

706 **Primary neuron lysis and western blot analysis**

707 Cells were washed 2x with ice-cold PBS and samples for the isolation of total proteins were
708 scraped in loading buffer containing dithiothreitol (50mM) and 2% sodium dodecyl sulfate
709 (SDS) to lyse the cells. The samples were triturated by a 21-gauge needle to sheer the DNA.
710 For analysis of cytosolic proteins, cells were lysed in 1%-Triton X-100 (Thermo Fisher
711 Scientific) in PBS supplemented with cOmplete protease inhibitor cocktail (Roche) and
712 PhosSTOP phosphatase inhibitors (Roche). To purify these whole-cell lysates, the lysates
713 were centrifuged at 14.000 g for 10 min at 4°C. The total protein content of the supernatant
714 was determined with the Pierce BCA protein assay kit (BCA) protein assay (Thermo Fisher
715 Scientific). All samples were boiled for 5 min at 95°C. An equal volume or amount of the
716 samples was loaded to a 4-15% Mini-Protean TGX stain-free precast polyacrylamide gels
717 (Bio-Rad) and Precision Plus ProteinTM All Blue Standards (Bio-Rad) was used as a ladder.
718 The total amount of protein on the gel was visualised using the Gel Doc EZ System (Bio-Rad)
719 and analysed using Image LabTM 6.0 (Bio-Rad). The total protein content was determined by
720 correcting for the measured area size. The samples were then transferred onto 0.2 µM
721 nitrocellulose membranes with the TransBlot Turbo transfer system and kit (both from Biorad).
722 The membranes were then blocked with 5% skimmed milk powder (Millipore) in TBS
723 containing 0.05% Tween (TBS-T) (Sigma-Aldrich) for 30 min at RT. Afterwards, the
724 membranes were incubated with primary antibody diluted in blocking buffer overnight at 4°C
725 (See table 1 for the dilutions of the primary antibodies). Subsequently, the membranes were
726 washed 4x 15 min in TBS-T whereafter the membranes were incubated with HRP-conjugated
727 secondary antibodies (DAKO) diluted in blocking buffer (1:2000) for 1 hour at RT. Last, the
728 membranes were washed 4x 15 min with TBS-T and submerged with SuperSignalTM West
729 Femto Maximum Sensitivity Substrate kit (Thermo Fisher Scientific). Membranes were
730 stripped for reblotting using ReBlot Plus Strong Antibody Stripping Solution (Merck). The
731 chemiluminescence was visualized with the Odessey Fc system (Li-Cor) and analysed using
732 Image Studio 6.0 software (Li-Cor). Band intensities were corrected for the background signal.

733

734 **Proteomics analysis of primary neurons**

735 **Sample preparation**

736 At day 15, media was aspirated and neurons were subjected to 2x gentle ice-cold PBS
737 washes. Neurons were then collected into 1.5 mL tubes using ice-cold PBS supplemented
738 with protease inhibitor (Roche). Samples were centrifuged for 5 min at 3000 x g at 4°C and
739 the remaining pellet was resuspended in 7 µL of 5x loading buffer containing 10% SDS, 0.25
740 M Tris pH 6.8, 0.1% bromophenol blue, 0.5 M DTT, 50% glycerol. Samples were stored at
741 −20°C until further use. A total of 14 samples from two independent experiments were
742 employed per condition.

743

744 **Protein in-gel digestion**

745 Cell lysates were incubated at 98°C for 6 min to denature the proteins followed by incubation
746 with 30% acrylamide/Bis Solution 37.5:1 (Bio-Rad) for 30 min at RT to block cysteine residues.
747 Samples were loaded onto 1 mm thick acrylamide gels. They were composed of 10%
748 acrylamide, 0.375 M Tris-HCl (pH 8.8), ultra-pure $H_2O$, 0.1% (w/v) APS and 6 µL N,N,N',N'-
749 tetramethylethylene-diamine (TEMED; Biorad) per gel. Proteins were allowed to migrate into
750 the gel by electrophoresis (120 V) for approximately 10 min. Peptides were extracted as
751 previously described[69]. Briefly, gels were fixed O/N in a solution containing 50% (v/v) ethanol
752 and 3% (v/v) phosphoric acid in $H_2O$ at RT and stained with Colloidal Coomassie Blue (34%
753 (v/v) methanol, 3% (v/v) phosphoric acid, 15% (w/v) ammonium sulphate and 0.1% (w/v)
754 Coomassie brilliant blue G-250 (Sigma-Aldrich)). Sample-containing lanes were separated
755 and cut in blocks. Gel fragments were destained in 50 mM $NH_4HCO_3$ (99% $NH_4HCO_3$, Fluka)
756 and 50% (v/v) acetonitrile (HPLC grade; JT Baker), dehydrated using 100% acetonitrile, re-
757 swell in 50 mM $NH_4HCO_3$ containing 10 µg/ml trypsin (sequence grade; Promega) and
758 incubated O/N in a humidified chamber at 37°C to facilitate protein digestion. Peptides were
759 extracted with a solution containing 0.1% (v/v) trifluoroacetic acid (Sigma-Aldrich) and 50%
760 (v/v) acetonitrile. Samples were dried using a SpeedVac (Eppendorf), and stored at −20°C
761 until LC-MS analysis.

762

763 **LC-MS analysis**

764 Samples (75 ng) were loaded into EvoTips (EV2003; Evosep) and run on a 15 cm x 75 µm,
765 1.9 µm Performance Column (EV112; Evosep) using the Evosep One LC system with 30
766 samples per day program. Peptides were electro-sprayed into the TimsTOF Pro 2 mass
767 spectrometer (Bruker Daltonics) and analysed with diaPASEF[70]. The MS was operated with

768 the following settings: scan range 100-1700 *m/z*, ion mobility 0.6 to 1.6 Vs/cm$^2$, ramp time 100
769 ms, accumulation time 100 ms and ramp rate 9.42 Hz.
770
771 **Data analysis**
772 Raw diaPASEF data from the TimsTOF Pro 2 were searched with a virtual spectral library
773 generated from the UniProt mouse proteome UP000000589_1090 using DIA-NN 1.8.1[71].
774 Deep-learning-based spectra and cross-run normalisation were activated. The maximum
775 number of missed cleavages was set to 1. The peptide length range was 7-30, the precursor
776 charge range to 2-4, the precursor m/z range to 300-1800 and the fragment ion m/z range to
777 200-800. A fixed modification of UniMod: 24, 71.0371 at C was used, which represents
778 acrylamide adduct. The precursor False Discovery Rate (FDR) was 1% (default). The rest of
779 the settings were used as default.
780
781 MS-DAP (v. 1.0)[72] was used for quality control and candidate discovery on the results obtained
782 from DIA-NN. Only peptides identified and quantified in at least 6 samples from each group
783 were included in the analysis. The batch effect of samples from different experiments was
784 removed by including the variable "batch" in MS-DAP. Normalisation of peptide abundance
785 values was applied and the MSqRob algorithm was used for differential analysis at the peptide
786 level using an FDR threshold of 5%.
787
788 GO and pathway analysis was performed using ShinyGO (v. 0.81)[73] with an FDR-adjusted p-
789 value threshold of 0.05. All detected proteins were used as background dataset. The glial
790 genes GFAP, OLIG1, OMG and AQP4 (as shown by squares in Fig.5a) were omitted for the
791 GO-term analysis. A minimum of 3 proteins belonging to the same pathway and a maximum
792 of 500 were considered to identify that pathway as a hit.
793
794 The mass spectrometry proteomics data have been deposited to the ProteomeXchange
795 Consortium via the PRIDE[74] partner repository with the dataset identifier PXD061887.
796

797 **Statistics**

798 GraphPad Prism 8.4.2 software was used for statistical analysis. Mean per neuron or mean
799 per well was used for the analysis of data obtained via confocal microscopy or high-throughput
800 microscopy, respectively. Data were normalised to the mean of the control condition, per
801 timepoint unless otherwise specified. Visual outliers in the pooled data were tested using the
802 ROUT method (Q = 1%) and excluded when significant. When applicable, a two-way ANOVA
803 was run followed by a Tukey's or Sidak's post-hoc test. Otherwise, the data were tested for

804 normality using the Shapiro-Wilk test. If the data were not normally distributed, the non-
805 parametric Mann-Whitney test for the comparison of two groups and a Kruskal-Wallis test
806 followed by a Dunn's multiple comparison post-hoc test for the comparison of more than two
807 groups were used. For normally distributed data, the conditions were grouped based on
808 experiments and a nested t-test was used for the comparison of two groups or a nested one-
809 way ANOVA followed by a Dunnett's multiple comparison of more than two groups. For the
810 comparison of tau+/GVB- and tau+/GVB+ neurons from the same well, a paired t-test was
811 used. For western blot analyses, an unpaired t-test was used to compare two groups or a two-
812 way ANOVA followed by a Tukey's post-hoc test was used when applicable. Only the most
813 relevant *P*-values were included in the figures. A *P*-value of $< 0.05$ was considered statistically
814 significant. $^{*}P < 0.05$, $^{**}P < 0.01$, $^{***}P < 0.001$, $^{****}P < 0.0001$ and ns: not significant.

## References


1. Spillantini, M. G. & Goedert, M. Tau pathology and neurodegeneration. *Lancet Neurol* **12**, 609–622 (2013).

2. Koren, S. A. *et al.* Tau drives translational selectivity by interacting with ribosomal proteins. *Acta Neuropathol* **137**, 571–583 (2019).

3. Jiang, L. *et al.* Interaction of tau with HNRNPA2B1 and N6-methyladenosine RNA mediates the progression of tauopathy. *Mol Cell* **81**, 4209-4227.e12 (2021).

4. Meier, S. *et al.* Pathological tau promotes neuronal damage by impairing ribosomal function and decreasing protein synthesis. *Journal of Neuroscience* **36**, 957–962 (2016).

5. Radford, H., Moreno, J. A., Verity, N., Halliday, M. & Mallucci, G. R. PERK inhibition prevents tau-mediated neurodegeneration in a mouse model of frontotemporal dementia. *Acta Neuropathol* **130**, 633–642 (2015).

6. Evans, H. T., Benetatos, J., van Roijen, M., Bodea, L. & Götz, J. Decreased synthesis of ribosomal proteins in tauopathy revealed by non-canonical amino acid labelling. *EMBO J* **38**, 1–15 (2019).

7. Nijholt, D. A. T., Van Haastert, E. S., Rozemuller, A. J. M., Scheper, W. & Hoozemans, J. J. M. The unfolded protein response is associated with early tau pathology in the hippocampus of tauopathies. *J Pathol* **226**, 693–702 (2012).

8. Hoozemans, J. J. M. *et al.* The unfolded protein response is activated in pretangle neurons in alzheimer's disease hippocampus. *American Journal of Pathology* **174**, 1241–1251 (2009).

9. Köhler, C. Granulovacuolar degeneration: a neurodegenerative change that accompanies tau pathology. *Acta Neuropathol* **132**, 339–359 (2016).

10. Ganz, A. B. *et al.* Neuropathology and cognitive performance in self-reported cognitively healthy centenarians. *Acta Neuropathol Commun* **6**, 64 (2018).

11. Zhang, M. *et al.* The correlation between neuropathology levels and cognitive performance in centenarians. *Alzheimer's & Dementia* **19**, 5036–5047 (2023).

12. Marta J. Koper *et al.* Necrosome complex detected in granulovacuolar degeneration is associated with neuronal loss in Alzheimer's disease. *Acta Neuropathol* **139**, 463–484 (2020).

13. Wiersma, V. I., Hoozemans, J. J. M. & Scheper, W. Untangling the origin and function of granulovacuolar degeneration bodies in neurodegenerative proteinopathies. *Acta Neuropathologica Communications 2020 8:1* **8**, 1–21 (2020).

14. Wiersma, V. I. *et al.* Granulovacuolar degeneration bodies are neuron-selective lysosomal structures induced by intracellular tau pathology. *Acta Neuropathol* **138**, 943–970 (2019).

15. Jorge-Oliva, M., Smits, J. F. M., Wiersma, V. I., Hoozemans, J. J. M. & Scheper, W. Granulovacuolar degeneration bodies are independently induced by tau and α-synuclein pathology. *Alzheimers Res Ther* **14**, 1–21 (2022).

855 16. Jorge-Oliva, M., van Weering, J. R. T. & Scheper, W. Structurally and Morphologically
856 Distinct Pathological Tau Assemblies Differentially Affect GVB Accumulation. *Int J Mol*
857 *Sci* **24**, 10865 (2023).

858 17. Lai, S. S. M., Ng, K. Y., Koh, R. Y., Chok, K. C. & Chye, S. M. Endosomal-lysosomal
859 dysfunctions in Alzheimer's disease: Pathogenesis and therapeutic interventions.
860 *Metabolic Brain Disease 2021 36:6* **36**, 1087–1100 (2021).

861 18. Nixon, R. A. & Rubinsztein, D. C. Mechanisms of autophagy–lysosome dysfunction in
862 neurodegenerative diseases. *Nature Reviews Molecular Cell Biology 2024 25:11* **25**,
863 926–946 (2024).

864 19. Kuijpers, M. *et al.* Neuronal Autophagy Regulates Presynaptic Neurotransmission by
865 Controlling the Axonal Endoplasmic Reticulum. *Neuron* **109**, 299-313.e9 (2021).

866 20. Vidal, R. L. *et al.* Targeting the UPR transcription factor XBP1 protects against
867 Huntington's disease through the regulation of FoxO1 and autophagy. *Hum Mol*
868 *Genet* **21**, 2245–2262 (2012).

869 21. Walton, K. M. *et al.* Selective inhibition of casein kinase 1ε minimally alters circadian
870 clock period. *Journal of Pharmacology and Experimental Therapeutics* **330**, 430–439
871 (2009).

872 22. Long, A., Zhao, H. & Huang, X. Structural Basis for the Interaction between Casein
873 Kinase 1 Delta and a Potent and Selective Inhibitor. (2011) doi:10.1021/jm201387s.

874 23. Yamoah, A. *et al.* Aggregates of RNA Binding Proteins and ER Chaperones Linked to
875 Exosomes in Granulovacuolar Degeneration of the Alzheimer's Disease Brain.
876 *Journal of Alzheimer's Disease* **75**, 139–156 (2020).

877 24. Kork, F. *et al.* Golgin A4 in CSF and granulovacuolar degenerations of patients with
878 Alzheimer disease. *Neurology* **91**, E1799–E1808 (2018).

879 25. Li, G., Yin, H. & Kuret, J. Casein Kinase 1 Delta Phosphorylates Tau and Disrupts Its
880 Binding to Microtubules. *Journal of Biological Chemistry* **279**, 15938–15945 (2004).

881 26. Roth, A. *et al.* Comprehensive Characterization of CK1δ-Mediated Tau
882 Phosphorylation in Alzheimer's Disease. *Front Mol Biosci* **9**, 1–16 (2022).

883 27. Batenburg, K. L., Kasri, N. N., Heine, V. M. & Scheper, W. Intraneuronal tau
884 aggregation induces the integrated stress response in astrocytes. *J Mol Cell Biol* **14**,
885 71 (2023).

886 28. Diane M. Milne, Paul Looby, and D. W. M. Catalytic Activity of Protein Kinase CK1d
887 (Casein Kinase 1d) Is Essential for Its Normal Subcellular Localization. *Exp Cell Res*
888 **263**, 43–54 (2001).

889 29. Lord, C. *et al.* Sequential interactions with Sec23 control the direction of vesicle traffic.
890 *Nature* **473**, 181–186 (2011).

891 30. Schmidt, E. K., Clavarino, G., Ceppi, M. & Pierre, P. SUnSET, a nonradioactive
892 method to monitor protein synthesis. *Nat Methods* **6**, 275–277 (2009).

893 31. Wolzak, K. *et al.* Neurons shift translational control to secure proteostatic resilience
894 during ER stress. *EMBO Journal* **41**, e110501 (2022).

895 32. Ryoo, H. D. The integrated stress response in metabolic adaptation. *Journal of*
896 *Biological Chemistry* **300**, (2024).

897 33. Ma, H. *et al.* Excitation–transcription coupling, neuronal gene expression and synaptic
898 plasticity. *Nature Reviews Neuroscience 2023 24:11* **24**, 672–692 (2023).

899 34. Minatohara, K., Akiyoshi, M. & Okuno, H. Role of Immediate-Early Genes in Synaptic
900 Plasticity and Neuronal Ensembles Underlying the Memory Trace. *Front Mol Neurosci*
901 **8**, (2016).

902 35. Jiang, Y. & Van Dongen, A. M. J. Selective Increase of Correlated Activity in Arc-
903 Positive Neurons after Chemically Induced Long-Term Potentiation in Cultured
904 Hippocampal Neurons. *eNeuro* **8**, ENEURO.0540-20.2021 (2021).

905 36. Koper, M. J. *et al.* LATE-NC aggravates GVD-mediated necroptosis in Alzheimer's
906 disease. *Acta Neuropathol Commun* **10**, 1–16 (2022).

907 37. Koper, M. J. *et al.* Inhibition of an Alzheimer's disease–associated form of necroptosis
908 rescues neuronal death in mouse models. *Sci Transl Med* **16**, (2024).

909 38. Ma, Y., McClatchy, D. B., Martínez-Bartolomé, S., Bamberger, C. & Yates, J. R.
910 Temporal Quantitative Profiling of Newly Synthesized Proteins during Aβ
911 Accumulation. *J Proteome Res* **20**, 763–775 (2021).

912 39. Chen, Q., Thorpe, J. & Keller, J. N. A-Synuclein Alters Proteasome Function, Protein
913 Synthesis, and Stationary Phase Viability. *Journal of Biological Chemistry* **280**,
914 30009–30017 (2005).

915 40. Deshpande, P. *et al.* Protein synthesis is suppressed in sporadic and familial
916 Parkinson's disease by LRRK2. *FASEB Journal* **34**, 14217–14233 (2020).

917 41. Garcia-Esparcia, P. *et al.* Altered machinery of protein synthesis is region- and stage-
918 dependent and is associated with α-synuclein oligomers in Parkinson's disease. *Acta*
919 *Neuropathol Commun* **3**, 1–25 (2015).

920 42. Moreno, J. A. *et al.* Sustained translational repression by eIF2α-P mediates prion
921 neurodegeneration. *Nature* **485**, 507–11 (2012).

922 43. Ma, T. *et al.* Suppression of eIF2α kinases alleviates Alzheimer's disease-related
923 plasticity and memory deficits. *Nat Neurosci* **16**, 1299–1305 (2013).

924 44. Halliday, M. *et al.* Repurposed drugs targeting eIF2α-P-mediated translational
925 repression prevent neurodegeneration in mice. *Brain* **140**, 1768–1783 (2017).

926 45. Halliday, M. *et al.* Partial restoration of protein synthesis rates by the small molecule
927 ISRIB prevents neurodegeneration without pancreatic toxicity. *Cell Death Dis* **6**,
928 e1672-9 (2015).

929 46. Moreno, J. A. *et al.* Oral Treatment Targeting the Unfolded Protein Response
930 Prevents Neurodegeneration and Clinical Disease in Prion-Infected Mice. *Sci Transl*
931 *Med* **5**, 206ra138-206ra138 (2013).

932 47. Richter, J. D. & Klann, E. Making synaptic plasticity and memory last: Mechanisms of
933 translational regulation. *Genes Dev* **23**, 1–11 (2009).

48. Costa-Mattioli, M., Sossin, W. S., Klann, E. & Sonenberg, N. Translational Control of Long-Lasting Synaptic Plasticity and Memory. *Neuron* Preprint at https://doi.org/10.1016/j.neuron.2008.10.055 (2009).

49. Di Lorenzo, F. *et al.* LTP-like cortical plasticity is associated with verbal memory impairment in Alzheimer's disease patients. *Brain Stimul* **12**, 148–151 (2019).

50. Shipton, O. A. *et al.* Tau protein is required for amyloid {beta}-induced impairment of hippocampal long-term potentiation. *J Neurosci* **31**, 1688–1692 (2011).

51. Aparicio, L. *et al.* Current Opinion on the Use of c-Fos in Neuroscience. *NeuroSci 2022, Vol. 3, Pages 687-702* **3**, 687–702 (2022).

52. Chen, Y., Wang, X., Xiao, B., Luo, Z. & Long, H. Mechanisms and Functions of Activity-Regulated Cytoskeleton-Associated Protein in Synaptic Plasticity. *Molecular Neurobiology 2023 60:10* **60**, 5738–5754 (2023).

53. Bramham, C. R., Worley, P. F., Moore, M. J. & Guzowski, J. F. The Immediate Early Gene Arc/Arg3.1: Regulation, Mechanisms, and Function. *The Journal of Neuroscience* **28**, 11760 (2008).

54. Korb, E. & Finkbeiner, S. Arc in synaptic plasticity: from gene to behavior. *Trends Neurosci* **34**, 591–598 (2011).

55. Kavanagh, T., Halder, A. & Drummond, E. Tau interactome and RNA binding proteins in neurodegenerative diseases. *Mol Neurodegener* **17**, 1–17 (2022).

56. Hondius, D. C. *et al.* The proteome of granulovacuolar degeneration and neurofibrillary tangles in Alzheimer's disease. *Acta Neuropathol* **141**, 341–358 (2021).

57. Nicklin, P. *et al.* Bidirectional Transport of Amino Acids Regulates mTOR and Autophagy. *Cell* **136**, 521–534 (2009).

58. Fulcher, L. J. & Sapkota, G. P. Functions and regulation of the serine/threonine protein kinase CK1 family: moving beyond promiscuity. *Biochemical Journal* **477**, 4603–4621 (2020).

59. Xu, P. *et al.* Structure, regulation, and (patho-)physiological functions of the stress-induced protein kinase CK1 delta (CSNK1D). *Gene* **715**, 144005–144031 (2019).

60. Cullati, S. N. *et al.* Substrate displacement of CK1 C-termini regulates kinase specificity. *Sci Adv* **10**, 5185 (2024).

61. Tanaka, C. *et al.* Hrr25 triggers selective autophagy–related pathways by phosphorylating receptor proteins. *Journal of Cell Biology* **207**, 91–105 (2014).

62. Pfaffenwimmer, T. *et al.* Hrr25 kinase promotes selective autophagy by phosphorylating the cargo receptor Atg19. *EMBO Rep* **15**, 862–870 (2014).

63. Wang, J. *et al.* Ypt1/Rab1 regulates Hrr25/CK1δ kinase activity in ER–Golgi traffic and macroautophagy. *Journal of Cell Biology* **210**, 273–285 (2015).

64. Li, Y. *et al.* Casein Kinase 1 Family Member CK1δ/Hrr25 Is Required for Autophagosome Completion. *Front Cell Dev Biol* **8**, 460 (2020).

65. Zemp, I. *et al.* CK1δ and CK1ε are components of human 40S subunit precursors required for cytoplasmic 40S maturation. *J Cell Sci* **127**, 1242–1253 (2014).

974 66. Ghalei, H. *et al.* Hrr25/CK1δ directed release of Ltv1 from pre-40S ribosomes is
975 necessary for ribosome assembly and cell growth. *J Cell Biol* **208**, 745–759 (2015).

976 67. Greer, Y. E. & Rubin, J. S. Casein kinase 1 delta functions at the centrosome to
977 mediate Wnt-3a–dependent neurite outgrowth. *Journal of Cell Biology* **192**, 993–1004
978 (2011).

979 68. Naldini, L. *et al.* In Vivo Gene Delivery and Stable Transduction of Nondividing Cells
980 by a Lentiviral Vector. *Science (1979)* **272**, 263–267 (1996).

981 69. Gonzalez-Lozano, M. A. & Koopmans, F. Data-Independent acquisition (SWATH)
982 mass spectrometry analysis of protein content in primary neuronal cultures. In: Li, K.
983 (eds) Neuroproteomics. *Neuromethods* **146**, 119–127 (2019).

984 70. Meier, F. *et al.* diaPASEF: parallel accumulation–serial fragmentation combined with
985 data-independent acquisition. *Nat Methods* **17**, 1229–1236 (2020).

986 71. Demichev, V., Messner, C. B., Vernardis, S. I., Lilley, K. S. & Ralser, M. DIA-NN:
987 neural networks and interference correction enable deep proteome coverage in high
988 throughput. *Nat Methods* **17**, 41–44 (2020).

989 72. Koopmans, F., Li, K., Klaasen, R. & Smit, A. The mass Spectrometry downstream
990 analysis pipeline (MS-DAP). 1.0. Github. https://github.com/ftwkoopmans/msdap
991 (2022).

992 73. Ge, S. X., Jung, D., Jung, D. & Yao, R. ShinyGO: A graphical gene-set enrichment
993 tool for animals and plants. *Bioinformatics* **36**, 2628–2629 (2020).

994 74. Perez-Riverol, Y. *et al.* The PRIDE database at 20 years: 2025 update. *Nucleic Acids*
995 *Res* **53**, D543–D553 (2025).

996

997

Figure 1

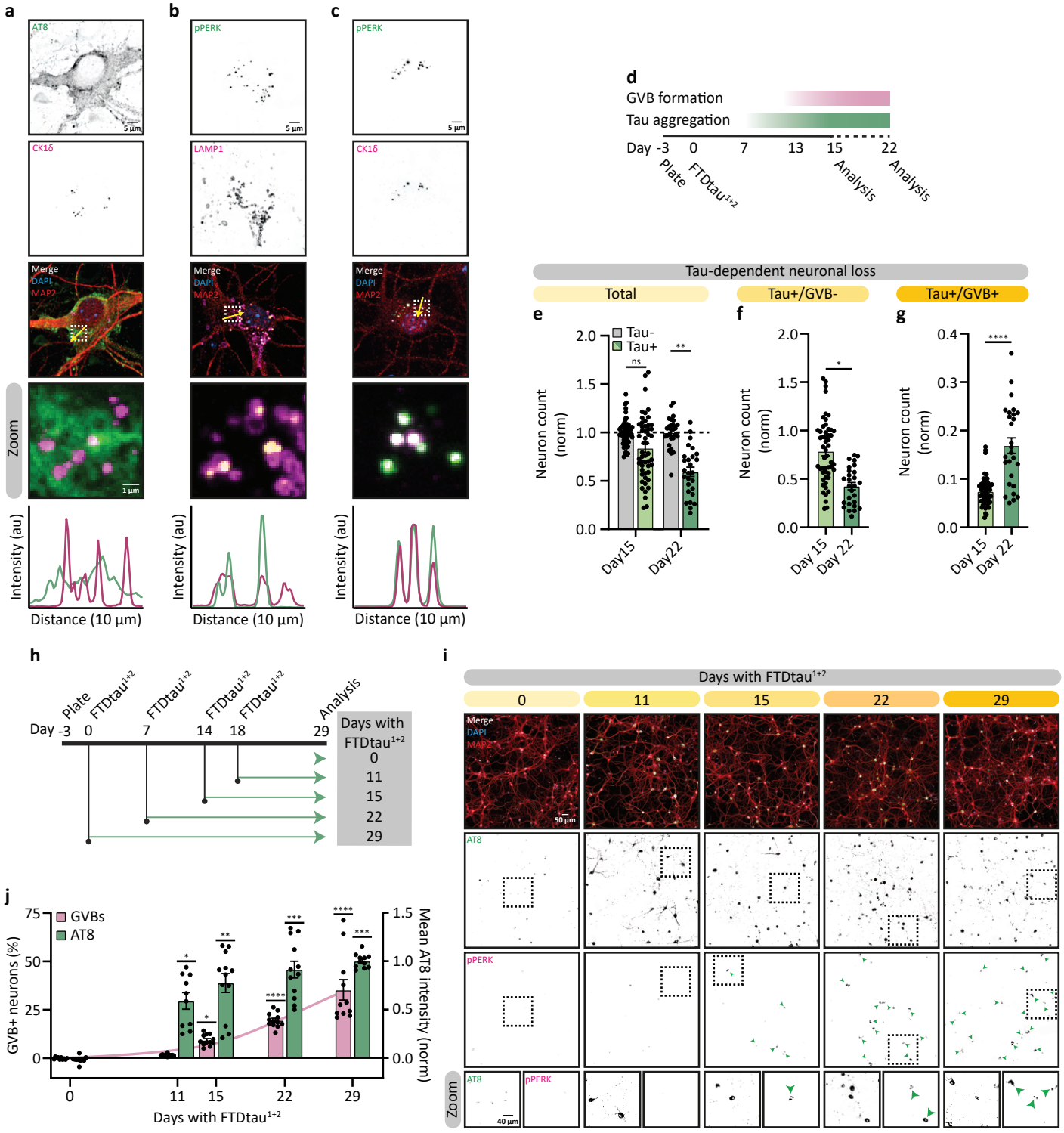
a
b
c
AT8
pPERK
pPERK
CK1δ
LAMP1
CK1δ
Merge
DAPI
MAP2
Zoom
Intensity (au)
Distance (10 µm)
d
GVB formation
Tau aggregation
Day -3
0
7
13
15
22
Plate
FTDtau1+2
Analysis
Analysis
Tau-dependent neuronal loss
Total
Tau+/GVB-
Tau+/GVB+
e
f
g
Tau-
Tau+
ns
**
*
****
Neuron count (norm)
Day15
Day22
Day 15
Day 22
h
Plate
FTDtau1+2
Analysis
Day -3
0
7
14
18
29
Days with FTDtau1+2
0
11
15
22
29
i
Days with FTDtau1+2
0
11
15
22
29
Merge
DAPI
MAP2
AT8
pPERK
Zoom
j
GVBs
AT8
GVB+ neurons (%)
Mean AT8 intensity (norm)
Days with FTDtau1+2

998 **Figure 1: GVB+ neurons are resilient to tau-induced neurodegeneration. a-c**
999 Representative confocal images of tau+/GVB+ neurons analysed at day 22. Neurons were
1000 immunostained for the phosphorylated tau marker AT8 (green) and the GVB marker CK1δ
1001 (magenta) (**a**), the GVB markers pPERK (green) and CK1δ (magenta) (**b**), pPERK (green)
1002 and lysosomal membrane marker LAMP1 (magenta) (**c**) and the dendrite marker MAP2 (red).
1003 The zoomed regions are indicated by dashed white squares and the yellow arrow represents
1004 the location of the line intensity profiles. **d** Schematic of the experimental timeline indicating
1005 the time of transduction with FTDtau$^{1+2}$, start of tau aggregation and GVB formation, analysis
1006 was at day 15 or 22. **e-g** Quantification of tau-induced neuronal loss (tau+; **e**), tau+/GVB- (**f**)
1007 or tau+/GVB+ (**g**) neurons analysed at day 15 or day 22, normalised to the mean number of
1008 tau- neurons per timepoint. For day 15, N=15 and n=57 (tau-) and 52 (tau+/GVB- and
1009 tau+/GVB+). For day 22, N=6 and n=27 (tau-) and 27 (tau+/GVB- and tau+/GVB+). A nested
1010 t-test (**e, f**) and a Mann-Whitney test (**g**) were used. **h** Schematic of the protocol used to assess
1011 the progression of tau aggregation and GVB+ formation by transduction with FTDtau$^{1+2}$ at the
1012 indicated points. **i** Representative high-content microscopy images at different FTDtau$^{1+2}$
1013 exposure durations as indicated. Neurons were immunostained for AT8 (green), MAP2 (red)
1014 and pPERK (magenta). The zoomed regions are indicated by dashed black squares. Green
1015 arrowheads indicate GVB+ neurons. **j** Quantification of the percentage GVB+ neurons and the
1016 mean AT8 immunofluorescence intensity normalized to 29 days FTDtau$^{1+2}$ exposure (1) and
1017 untransduced (0). Single datapoints represent one well. N=4 and n=10, 10, 12, 12 and 11 for
1018 0, 11, 15, 22 and 29 days with FTDtau$^{1+2}$, respectively. A nested one-way ANOVA followed by
1019 a Dunnett's post-hoc test (AT8 intensity) and a Kruskal-Wallis test followed by a Dunn's post-
1020 hoc test (GVB%) were used. Nuclei were visualised by DAPI (blue) and separate channels
1021 are shown in greyscale (**a-c, i**). Single datapoints represent one well (**e-g, j**). Data are
1022 presented as mean ± s.e.m. *P*-values are indicated: **P* < 0.05, ***P* < 0.01, ****P* < 0.001,
1023 *****P* < 0.0001 and ns: not significant.

Figure 2

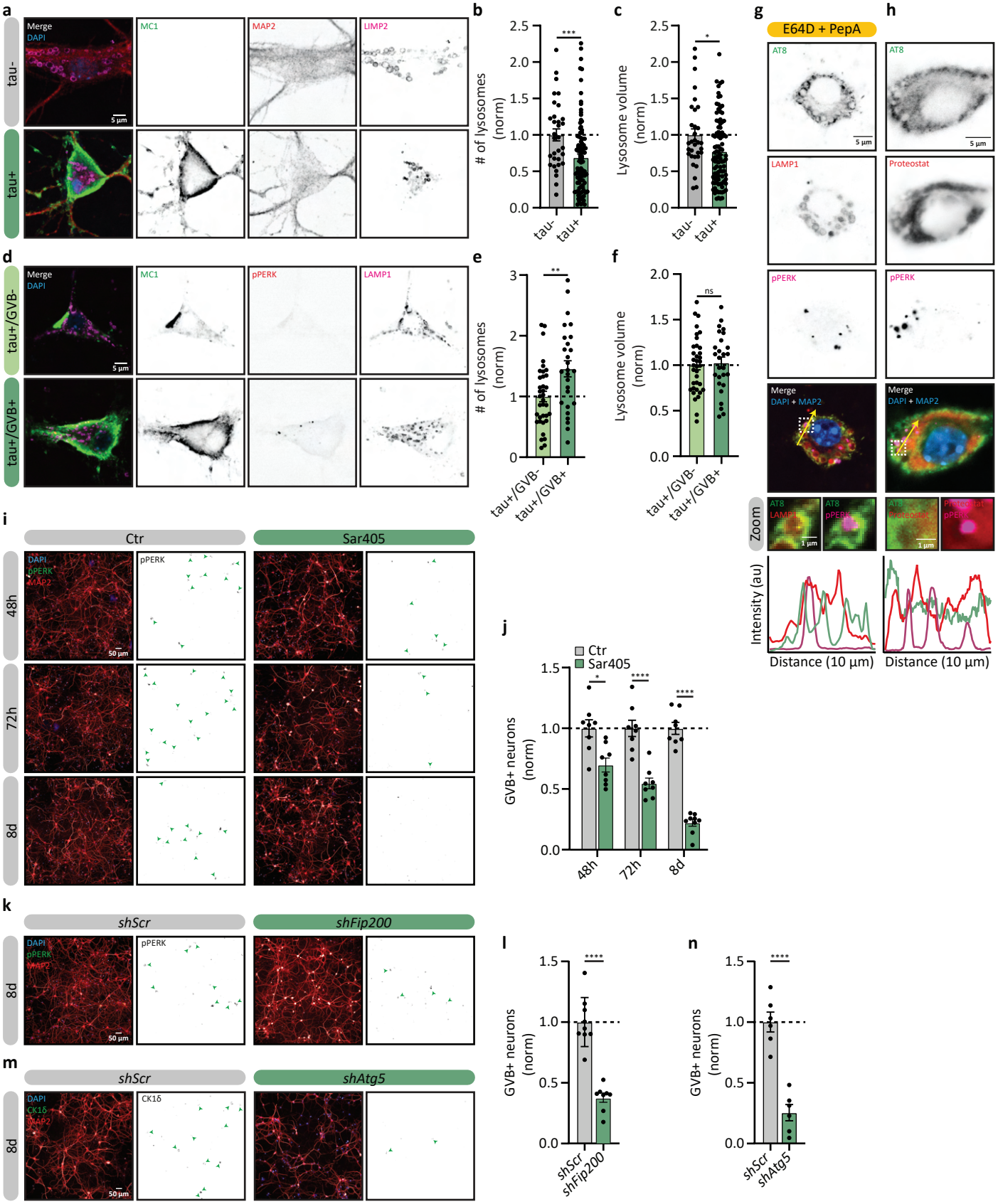
a
tau-
tau+
Merge
DAPI
MC1
MAP2
LIMP2
5 µm
b
# of lysosomes (norm)
tau-
tau+
c
Lysosome volume (norm)
d
tau+/GVB-
tau+/GVB+
pPERK
LAMP1
e
f
ns
g
E64D + PepA
AT8
LAMP1
h
Proteostat
Merge
DAPI + MAP2
Zoom
1 µm
Intensity (au)
Distance (10 µm)
i
Ctr
Sar405
48h
72h
8d
50 µm
j
GVB+ neurons (norm)
k
shScr
shFip200
l
n
m
shAtg5
CK1δ

1024 **Figure 2: GVB formation requires basal autophagy. a** Representative confocal images of
1025 tau- or tau+ neurons analysed at day 15. Neurons were immunostained for the pathological
1026 tau marker MC1 (green), the dendrite marker MAP2 (red) and the lysosomal membrane
1027 marker LIMP2 (magenta). **b, c** Single cell quantification of the number of LIMP2+ lysosomes
1028 in the soma (**b**) and lysosomal volume (**c**) in tau- and tau+ neurons analysed at day 15. Data
1029 were normalised to tau- neurons. N=3 and n=32 (tau-) and 97 (tau+). A Mann-Whitney test (**b,**
1030 **c**) was used. **d** Representative confocal images of tau+/GVB- and tau+/GVB+ neurons at day
1031 15, immunostained for MC1 (green), the GVB-marker pPERK (red) and the lysosomal
1032 membrane marker LAMP1 (magenta). **e, f** Single cell quantification of the number of LAMP1+
1033 lysosomes in the soma including (**e**) and lysosomal volume (**f**) in tau+/GVB- and tau+/GVB+
1034 neurons analysed at day 15. Data were normalised to the mean of tau+/GVB- neurons. N=3
1035 and n=36 (tau+/GVB-) and 27 (tau+/GVB+). A Mann-Whitney test (**e, f**) was used. **g**
1036 Representative confocal images of tau+/GVB+ neurons treated with lysosomal inhibitors E64D
1037 and PepstatinA (PepA) for 24h analysed at day 15. Neurons were immunostained for the
1038 phosphorylated tau marker AT8 (green), LAMP1 (red), pPERK (magenta) and MAP2 (blue).
1039 **h** Representative confocal images of tau+/GVB+ neurons analysed at day 15. Neurons were
1040 treated with Proteostat (red) to detect aggregated proteins and immunostained for AT8
1041 (green), pPERK (magenta) and MAP2 (blue). **i** Representative high-content microscopy
1042 images of tau+ neurons treated without or with the VPS34 chemical inhibitor Sar405 for 48h,
1043 72h or 8d analysed at day 15. Neurons were immunostained for MAP2 (red) and pPERK
1044 (green). **j** Quantification of the percentage of pPERK+ GVB+ neurons upon Sar405 treatment
1045 normalised to untreated per timepoint at day 15. N=3 and n=9 and 8 (48h), n=8 and 8 (72h),
1046 n=8 and 9 (8d), Ctr and Sar405, respectively. A nested t-test (48h and 72h) and a Mann-
1047 Whitney test (8d) were used. **k, m** Representative high-content microscopy images of tau+
1048 neurons transduced with a control (*shScr*), shRNA targeting *Fip200* (*shFip200*; **k**) or *Atg5*
1049 (*shAtg5;* **m**) 8d before analysis at day 15. Neurons were immunostained for MAP2 (red) and
1050 pPERK (**k**) or CK1δ (**m**) (green). **l, n** Quantification of the the percentage of pPERK+ (**l**) or
1051 CK1δ+ (**n**) GVB+ neurons upon *Fip200* (**l**) and *Atg5* knock-down (KD) (**n**) normalised to *shScr*.
1052 N=3 and n=9 and 8 (*Fip200* KD), n=6 and 6 (*Atg5* KD), *shScr* and *shFip200* or *shAtg5*,
1053 respectively. A nested t-test was used (**l, n**). Nuclei were visualised by DAPI (blue) and
1054 separate channels are shown in greyscale (**a, d, g, h, i, k, m**). Zoomed regions are indicated
1055 by a dashed white square and the yellow arrow represents the location of the line intensity
1056 profile (**g, h**). Green arrowheads indicate single GVB+ neurons (**i, k, m**). Single datapoints
1057 represent one well (**j, l, m**). Data are presented as mean ± s.e.m. *P*-values are indicated: **P* <
1058 0.05, ***P* < 0.01, ****P* < 0.001, *****P* < 0.0001 and ns: not significant.

Figure 3

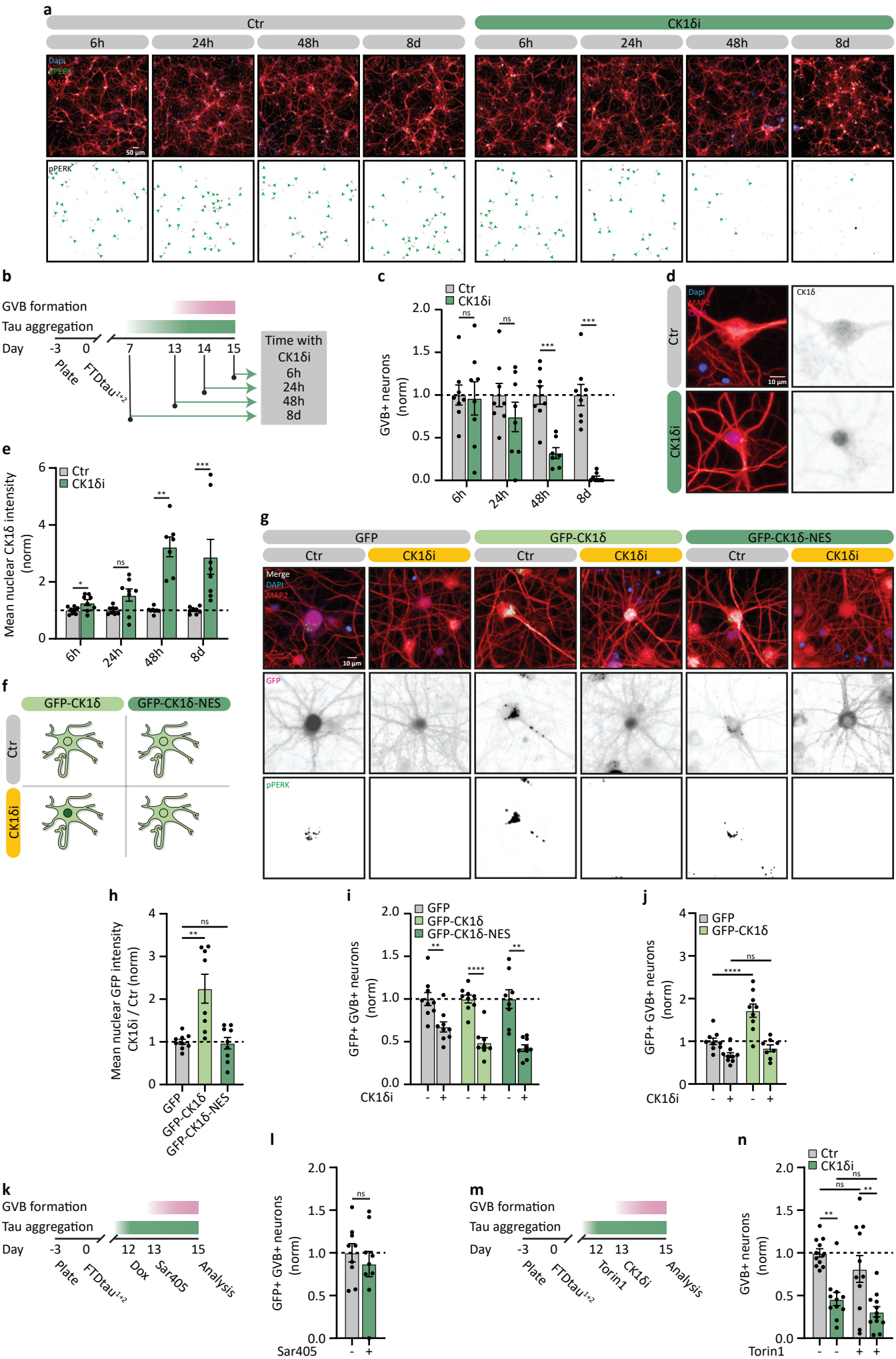
a
Ctr
CK1δi
6h
24h
48h
8d
Dapi
pPERK
MAP2
50 µm
b
GVB formation
Tau aggregation
Day
-3
0
7
13
14
15
Plate
FTDtau1+2
Time with CK1δi
6h
24h
48h
8d
c
Ctr
CK1δi
GVB+ neurons (norm)
ns
***
d
Ctr
CK1δi
Dapi
MAP2
CK1δ
10 µm
e
Mean nuclear CK1δ intensity (norm)
*
**
***
f
GFP-CK1δ
GFP-CK1δ-NES
g
GFP
GFP-CK1δ
GFP-CK1δ-NES
Merge
DAPI
MAP2
GFP
pPERK
h
Mean nuclear GFP intensity CK1δi / Ctr (norm)
i
GFP+ GVB+ neurons (norm)
****
j
k
Sar405
Dox
Analysis
l
m
Torin1
n

1059 **Figure 3: CK1δ is a key regulator for the formation of GVBs**. **a** Representative high-
1060 content microscopy images of tau+ neurons without or with CK1$\delta_i$ for 6h, 24h, 48h or 8d
1061 analysed at day 15. Neurons were immunostained for the dendrite marker MAP2 (red) and
1062 the GVB marker pPERK (green). Green arrowheads indicate single GVB+ neurons. **b**
1063 Schematic of the timeline of CK1$\delta_i$. **c, e** Quantification of the percentage of pPERK+ GVB+
1064 neurons (**c**) or mean nuclear CK1δ intensity (**e**) upon CK1$\delta_i$ treatment analysed at day 15
1065 normalised to untreated per timepoint. N=3 and n=8 and 8 (6h), 8 and 8 (24h), 8 and 7 (48h),
1066 8 and 8 (8d), for Ctr and CK1$\delta_i$, respectively. A nested t-test (6h, 24h and 48h; **c, e**) and a
1067 Mann-Whitney test (8d; **c, e**) were used. **d** Representative high-content microscopy images of
1068 tau+ neurons treated without or with CK1$\delta_i$ for 48h analysed at day 15. Neurons were
1069 immunostained for MAP2 (red) and CK1δ (magenta). **f** Schematic representation of
1070 subcellular localization of GFP-CK1δ and GFP-CK1δ-NES in the absence and presence of
1071 CK1$\delta_i$. **g** Representative high-content microscopy images of tau+ neurons transduced with
1072 GFP, GFP-CK1δ or GFP-CK1δ-NES without or with CK1$\delta_i$ for 48h analysed at day 22. Shown
1073 are GFP signal (magenta) and immunofluorescent signal for MAP2 (red) and pPERK (green).
1074 **h** Quantification of mean nuclear GFP signal of neurons transduced with GFP, GFP-CK1δ or
1075 GFP-CK1δ-NES upon 48h of CK1$\delta_i$ treatment in GFP-selected neurons analysed at day 22.
1076 First, the nuclear GFP intensity was normalised per group upon CK1$\delta_i$, after which it was
1077 normalised to the response in GFP-transduced neurons. N=3 and n=9 (GFP), 8 (GFP-CK1δ),
1078 9 (GFP-CK1δ-NES). A Kruskal-Wallis test followed by a Dunn's post-hoc test was used. **i**
1079 Quantification of the percentage of pPERK+ GVB+ neurons of neurons transduced with GFP,
1080 GFP-CK1δ or GFP-CK1δ-NES upon 48h of CK1$\delta_i$ treatment in GFP-selected neurons
1081 analysed at day 22 normalised to untreated per group. N=3 and n=9 and 9 (GFP), 9 and 8
1082 (GFP-CK1δ), 9 and 9 (GFP-CK1δ-NES), for Ctr and CK1$\delta_i$, respectively. A nested t-test was
1083 used. **j** Quantification of the percentage of pPERK+ GVB+ neurons transduced with GFP or
1084 GFP-CK1δ, upon 48h of CK1$\delta_i$ treatment in GFP-selected neurons analysed at day 22 and
1085 normalised to untreated GFP-transduced neurons. N=3 and n=9 and 9 (GFP), 9 and 8 (GFP-
1086 CK1δ), for Ctr and CK1$\delta_i$, respectively. A two-way ANOVA followed by a Sidak's post-hoc test
1087 was used. **k** Schematic of the timeline of induction of CK1δ expression (Dox) and inhibition of
1088 autophagy (Sar405). **l** Quantification of the percentage of GFP+/GVB+ neurons transduced
1089 with Dox-GFP-CK1δ and treated with Dox for 72h, without or with Sar405 for 48h, analysed at
1090 day 15 and normalised to untreated. GVBs were defined using Dox-GFP-CK1δ as the GVB-
1091 marker. N=3 and n=9. A nested t-test was used. **m** Schematic of the timeline of induction of
1092 autophagy (Torin1) and CK1$\delta_i$. **n** Quantification of the percentage of pPERK+ GVB+ neurons
1093 upon CK1$\delta_i$ treatment without or with prior Torin1 treatment analysed at day 15 normalised to
1094 untreated. N=4 and n=11. A two-way ANOVA test followed by a Tukey's post-hoc test was
1095 used. Nuclei were visualised by DAPI (blue) and separate channels are shown in greyscale

1096 (**a, d, g**). Single datapoints represent one well (**c, e, h-j, l, n**). Data are presented as
1097 mean ± s.e.m. *P*-values are indicated: *$P < 0.05$, **$P < 0.01$, ***$P < 0.001$, ****$P < 0.0001$ and
1098 ns: not significant.

Figure 4

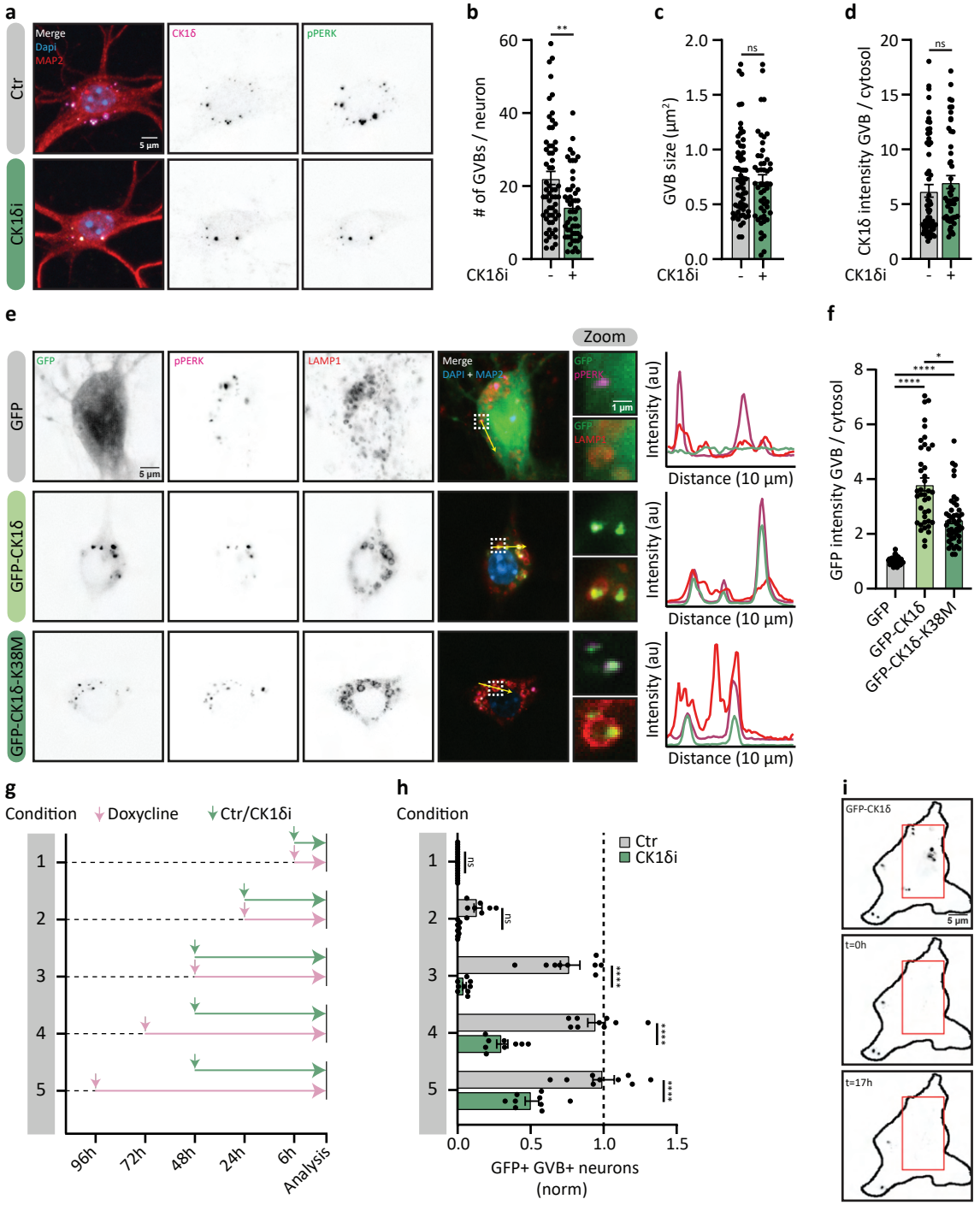
a
Ctr
CK1δi
Merge
Dapi
MAP2
CK1δ
pPERK
5 µm
b
# of GVBs / neuron
CK1δi
c
GVB size (µm²)
d
CK1δ intensity GVB / cytosol
e
Zoom
GFP
GFP-CK1δ
GFP-CK1δ-K38M
LAMP1
Merge
DAPI + MAP2
1 µm
Intensity (au)
Distance (10 µm)
f
GFP intensity GVB / cytosol
GFP
GFP-CK1δ
GFP-CK1δ-K38M
g
Condition
Doxycline
Ctr/CK1δi
96h
72h
48h
24h
6h
Analysis
h
Condition
Ctr
CK1δi
GFP+ GVB+ neurons
(norm)
i
GFP-CK1δ
t=0h
t=17h

1099 **Figure 4: CK1δ accumulation in GVBs marks the appearance of GVBs**. **a** Representative
1100 confocal images of tau+/GVB+ neurons without or with CK1$\delta_i$ for 48h analysed at day 22
1101 (maximum intensity projected Z-stacks). Neurons were immunostained for the GVB markers
1102 CK1δ (magenta) and pPERK (green) and the dendrite marker MAP2 (red). **b-d** Single cell
1103 quantification of number of GVBs per neuron (**b**), single GVB size (**c**) and the ratio of CK1δ
1104 intensity in the GVB over the cytosol (**d**) of tau+/GVB+ neurons without or with CK1$\delta_i$ for 48h
1105 analysed at day 22. N=3 and n=61 and 57, for Ctr and CK1$\delta_i$, respectively. A Mann-Whitney
1106 test (**b-d**) was used. **e** Representative confocal images of tau+/GVB+ neurons analysed at
1107 day 22. Neurons were transduced with GFP, GFP-CK1δ or GFP-CK1δ-K38M. The neurons
1108 were immunostained for pPERK (magenta), the lysosomal membrane marker LAMP1 (red)
1109 and MAP2 (blue). The zoomed regions are indicated by dashed white squares and the yellow
1110 arrow represents the location of the line intensity profiles. **f** Single cell quantification of the
1111 ratio of GFP, GFP-CK1δ or GFP-CK1δ-K38M intensity in the pPERK+ GVBs over the cytosol
1112 analysed at day 22. N=3 and n=42 (GFP), 40 (GFP-CK1δ), 45 (GFP-CK1δ-K38M). A two-way
1113 ANOVA followed by a Tukey's post-hoc test was used. **g** Schematic overview of tau+ neurons
1114 transduced with Dox-GFP-CK1δ treated with doxycycline (Dox) for 6h, 24h, 48h, 72h or 96h
1115 as indicated by the pink arrow and without or with CK1$\delta_i$ for 6h, 24h or 48h indicated by the
1116 green arrow. **h** Quantification of the percentage of GFP+/GVB+ neurons treated with Dox and
1117 without or with CK1$\delta_i$ according to the conditions specified in **g** normalised to control neurons
1118 treated for 96h with Dox analysed at day 22. GVBs were defined using Dox-GFP-CK1δ as the
1119 GVB-marker. Single datapoints represent one well. N=3 and n=8 and 8 (condition 2), 9 and 9
1120 (for the other conditions), Ctr and CK1$\delta_i$, respectively. **i** Representative live confocal images
1121 of tau+/GVB+ neurons transduced with GFP-CK1δ and followed over time after FRAP. Shown
1122 are cells directly after FRAP (t=0h) and at the end of the experiment (t=17h) is shown. The
1123 red square indicates the region that was exposed to FRAP. Nuclei were visualised by DAPI
1124 (blue) and separate channels are shown in greyscale (**a, e**). Data are presented as
1125 mean ± s.e.m. *P*-values are indicated: $^{*}P < 0.05$, $^{**}P < 0.01$, $^{****}P < 0.0001$ and ns: not
1126 significant.

Figure 5

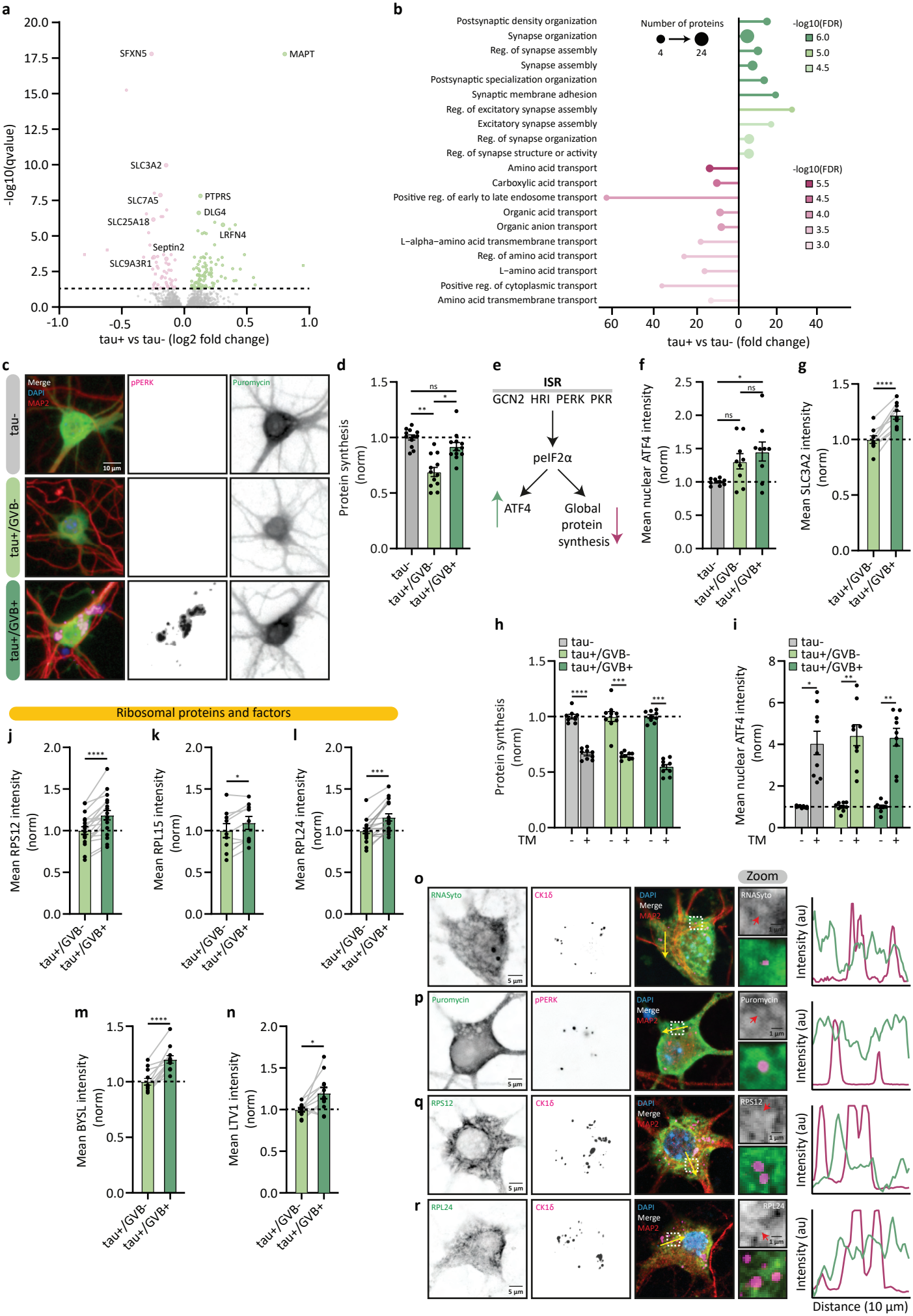
a
-log10(qvalue)
tau+ vs tau- (log2 fold change)
SFXN5
MAPT
SLC3A2
SLC7A5
PTPRS
DLG4
SLC25A18
LRFN4
Septin2
SLC9A3R1
b
Number of proteins
4
24
-log10(FDR)
6.0
5.0
4.5
5.5
4.5
4.0
3.5
3.0
Postsynaptic density organization
Synapse organization
Reg. of synapse assembly
Synapse assembly
Postsynaptic specialization organization
Synaptic membrane adhesion
Reg. of excitatory synapse assembly
Excitatory synapse assembly
Reg. of synapse organization
Reg. of synapse structure or activity
Amino acid transport
Carboxylic acid transport
Positive reg. of early to late endosome transport
Organic acid transport
Organic anion transport
L-alpha-amino acid transmembrane transport
Reg. of amino acid transport
L-amino acid transport
Positive reg. of cytoplasmic transport
Amino acid transmembrane transport
tau+ vs tau- (fold change)
c
tau-
tau+/GVB-
tau+/GVB+
Merge
DAPI
MAP2
pPERK
Puromycin
10 µm
d
Protein synthesis (norm)
ns
**
*
e
ISR
GCN2 HRI PERK PKR
peIF2α
ATF4
Global protein synthesis
f
Mean nuclear ATF4 intensity (norm)
g
Mean SLC3A2 intensity (norm)
****
h
Protein synthesis (norm)
TM
i
Mean nuclear ATF4 intensity (norm)
Ribosomal proteins and factors
j
Mean RPS12 intensity (norm)
k
Mean RPL15 intensity (norm)
l
Mean RPL24 intensity (norm)
m
Mean BYSL intensity (norm)
n
Mean LTV1 intensity (norm)
o
Zoom
RNASyto
CK1δ
DAPI
Merge
MAP2
5 µm
1 µm
Intensity (au)
p
Puromycin
pPERK
q
RPS12
r
RPL24
Distance (10 µm)

1127 **Figure 5: GVB+ neurons are resilient to tau-induced protein synthesis impairment. a**
1128 Volcano plot showing significantly upregulated (green) and downregulated (pink) proteins in
1129 tau+ neurons (q-value < 0.05) analysed at day 15. See Methods for details. **b** Most significant
1130 terms resulting from the GO enrichment analysis of significantly upregulated (green) and
1131 downregulated (pink) proteins in tau+ neurons. The circle size at the tip of the bar represents
1132 the number of significant proteins involved in the process and the colour intensity is indicative
1133 of the significance of the GO term. See Methods for details. **c** Representative high-content
1134 microscopy images showing tau-, tau+/GVB- and tau+/GVB+ neurons analysed at day 22.
1135 Neurons were treated for 15min with puromycin and were immunostained for puromycinilated
1136 proteins (green), the dendrite marker MAP2 (red) and the GVB marker pPERK (magenta). **d**
1137 Quantification of puromycin intensity as a measure for *de novo* protein synthesis in tau-,
1138 tau+/GVB- and tau+/GVB+ (pPERK based) neurons analysed at day 22 normalised to tau-
1139 neurons. N=4 and n=12. A nested one-way ANOVA followed by a Tukey's post-hoc test was
1140 used. **e** Schematic overview of the integrated stress response (ISR). **f** Quantification of mean
1141 nuclear ATF4 intensity in tau-, tau+/GVB- and tau+/GVB+ (CK1δ based) neurons at day 22
1142 normalised to tau-. Single datapoints represent one well. N=3 and n=9. A nested one-way
1143 ANOVA followed by a Tukey's post-hoc test was used. **g** Quantification of SLC3A2 somatic
1144 intensity in tau+/GVB- and tau+/GVB+ (CK1δ based) neurons analysed at day 22. N=3 and
1145 n=9. A paired t-test was used. **h** Quantification of puromycin intensity as a measure for *de*
1146 *novo* protein synthesis in tau-, tau+/GVB- and tau+/GVB+ (pPERK based) neurons treated
1147 with TM for 24h analysed at day 22 normalised to each group. N=3 and n= 8 and 9 (tau-), 9
1148 and 9 (tau+/GVB-), 9 and 9 (tau+/GVB+), for Ctr and TM, respectively. A nested t-test was
1149 used. **i** Quantification of mean nuclear ATF4 intensity in tau-, tau+/GVB- and tau+/GVB+
1150 (CK1δ based) neurons treated with TM for 24h analysed at day 22 normalised to each group.
1151 N=3 and n=9. A nested t-test was used. **j-n** Quantification of somatic intensities in tau+/GVB-
1152 and tau+/GVB+ (CK1δ based) neurons analysed at day 22 for 40S ribosomal protein S12
1153 (RPS12) (**j**), 60S ribosomal protein L15 (RPL15) (**k**), 60S ribosomal protein L24 (RPL24) (**l**)
1154 and ribosome biogenesis factors BYSL (**m**) and LTV1 (**n**). RPS12 (**j**): N=6 and n=18. RPL15
1155 (**k**): N=3 and n=9. RPL24 (**l**): N=6 and n=18. BYSL (**m**): N=4 and n=11. LTV1 (**n**): N=4 and
1156 n=11. A paired t-test (**j-n**) was used. **o-r**, Representative confocal images of tau+/GVB+
1157 neurons analysed at day 22. Neurons were treated with SYTO RNASelect to visualise RNA
1158 for 4h (green) and immunostained for CK1δ (magenta) (**o**), puromycin (green) and pPERK
1159 (magenta) (**p**), RPS12 (green) and CK1δ (magenta) (**q**) and RPL24 (green) and CK1δ
1160 (magenta) (**r**) and MAP2 (red). Nuclei were visualised by DAPI (blue). The zoomed regions
1161 are indicated by dashed white squares and the yellow arrow represents the location of the line
1162 intensity profiles. The red arrow points to a single GVB core. Nuclei were visualised by DAPI
1163 (blue) and separate channels are shown in greyscales (**c, o-r**). Single datapoints represent

one well (**d, f, g, h, i, j-n**). Data are presented as mean ± s.e.m. *P*-values are indicated: *$P < 0.05$, **$P < 0.01$, ***$P < 0.001$, ****$P < 0.0001$ and ns: not significant.

# Figure 6

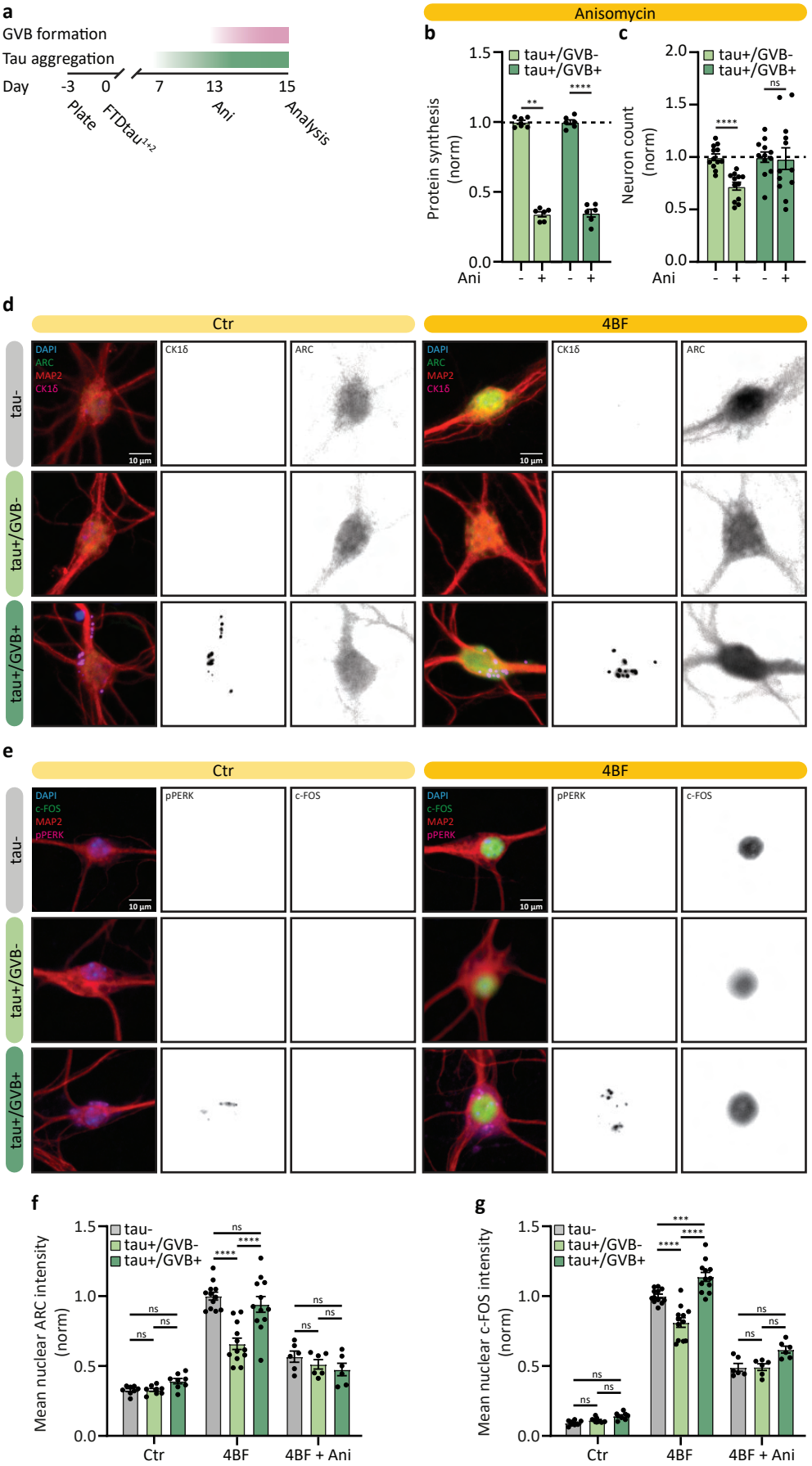
a
GVB formation
Tau aggregation
Day
-3
0
7
13
15
Plate
FTDtau1+2
Ani
Analysis
Anisomycin
b
Protein synthesis (norm)
tau+/GVB-
tau+/GVB+
Ani
c
Neuron count (norm)
d
Ctr
4BF
tau-
tau+/GVB-
tau+/GVB+
DAPI
ARC
MAP2
CK1δ
10 µm
e
c-FOS
pPERK
f
Mean nuclear ARC intensity (norm)
Ctr
4BF
4BF + Ani
g
Mean nuclear c-FOS intensity (norm)

1166 **Figure 6: GVB+ neurons fully retain the capacity to control LTP-regulated protein**
1167 **synthesis in the presence of tau pathology. a** Schematic of the timeline of protein synthesis
1168 inhibition using anisomycin (Ani). **b** Quantification of puromycin intensity as a measure for *de*
1169 *novo* protein synthesis in tau+/GVB- and tau+/GVB+ (pPERK based) neurons treated with Ani
1170 for 48h analysed at day 15 and normalised to untreated per group. N=3 and n=6. A Mann-
1171 Whitney test (tau+/GVB-) and a nested t-test (tau+/GVB+) were used. **c** Quantification of
1172 neuron number of tau+/GVB- and tau+/GVB+ (pPERK based) neurons treated with
1173 anisomycin for 48h analysed at day 15 and normalised to untreated per group. N=4 and n=12.
1174 A nested t-test was used. **d, e** Representative high-content microscopy images of tau-,
1175 tau+/GVB- and tau+/GVB+ neurons treated without or with 4BF (see Methods) for 4h. Neurons
1176 were immunostained for IEGs ARC (**d**) or c-FOS (**e**), the dendrite marker MAP2 (red) and the
1177 GVB marker CK1δ (magenta). Nuclei were visualised by DAPI (blue). Separate channels are
1178 shown in greyscales. **f, g** Quantification of mean nuclear ARC (**f**) or c-FOS (**g**) in tau-,
1179 tau+/GVB- and tau+/GVB+ (CK1δ (**f**) or pPERK (**g**) based) neurons upon 4BF-dependent
1180 LTP-induction treated without or with anisomycin before LTP-induction normalised to tau-
1181 LTP-induced response. Single datapoints represent one well. N=4 (Ctr and 4BF) and 3 (4BF
1182 + Ani) and n=8, 8 and 8 (Ctr), 12, 12 and 12 (4BF), 6, 6 and 6 (4BF + Ani), for tau-, tau+/GVB-
1183 and tau+/GVB+, respectively. A two-way ANOVA test followed by a post-hoc Tukey's test (**f,**
1184 **g**) was used. Single datapoints represent one well (**b, c, f, g**). Data are presented as
1185 mean ± s.e.m. *P*-values are indicated: $^{**}P < 0.01$, $^{***}P < 0.001$, $^{****}P < 0.0001$ and ns: not
1186 significant.

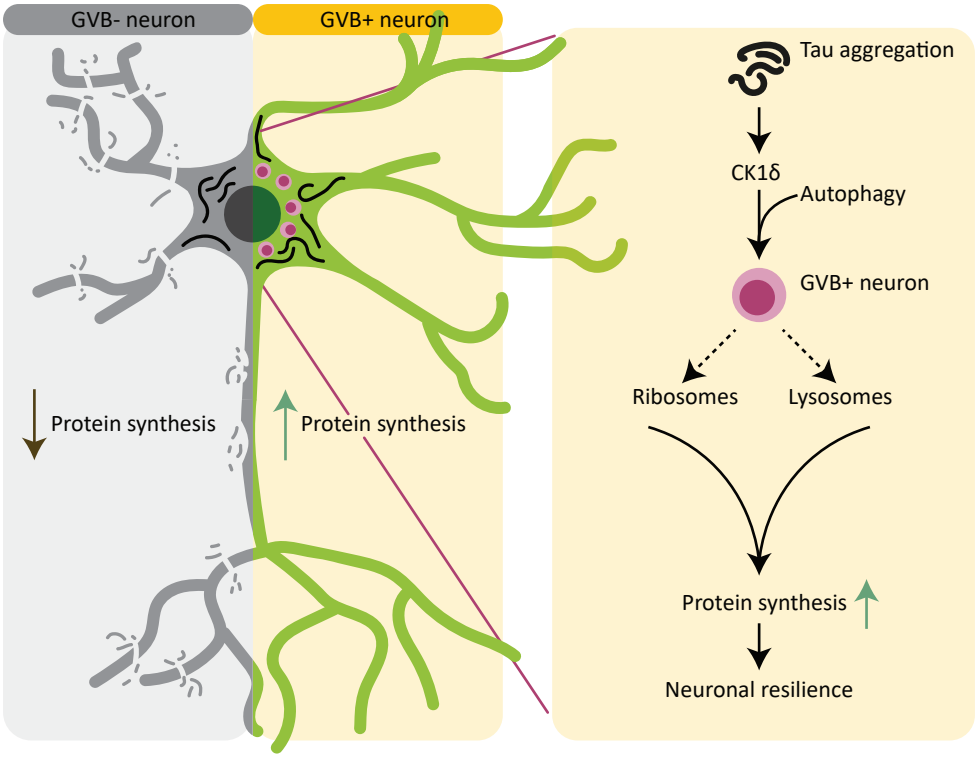


1187 **Figure 7: Model for the resilience to tau pathology-mediated neurodegeneration by GVB**
1188 **formation**. Intraneuronal tau aggregation impairs protein synthesis and ultimately leads to
1189 neuron loss. In a subset of neurons, CK1δ activation drives GVB formation in an autophagy-
1190 dependent manner. GVB+ neurons are resilient to tau-induced protein synthesis impairment
1191 and neurodegeneration. This resilience is facilitated by enhanced ribosomal and lysosomal
1192 content, which supports protein synthesis by increasing the protein synthesis machinery as
1193 well as the free amino acid pool. This allows GVB+ neurons (in contrast to GVB- neurons) to
1194 fully retain the capacity to induce the LTP-induced synthesis of IEGs in the presence of tau
1195 pathology, unlike GVB- neurons. Our data identify CK1δ-induced GVB formation as an
1196 intrinsic neuron-specific resilience mechanism that provides neuronal protection against tau
1197 pathology.

# Extended Data Fig.1

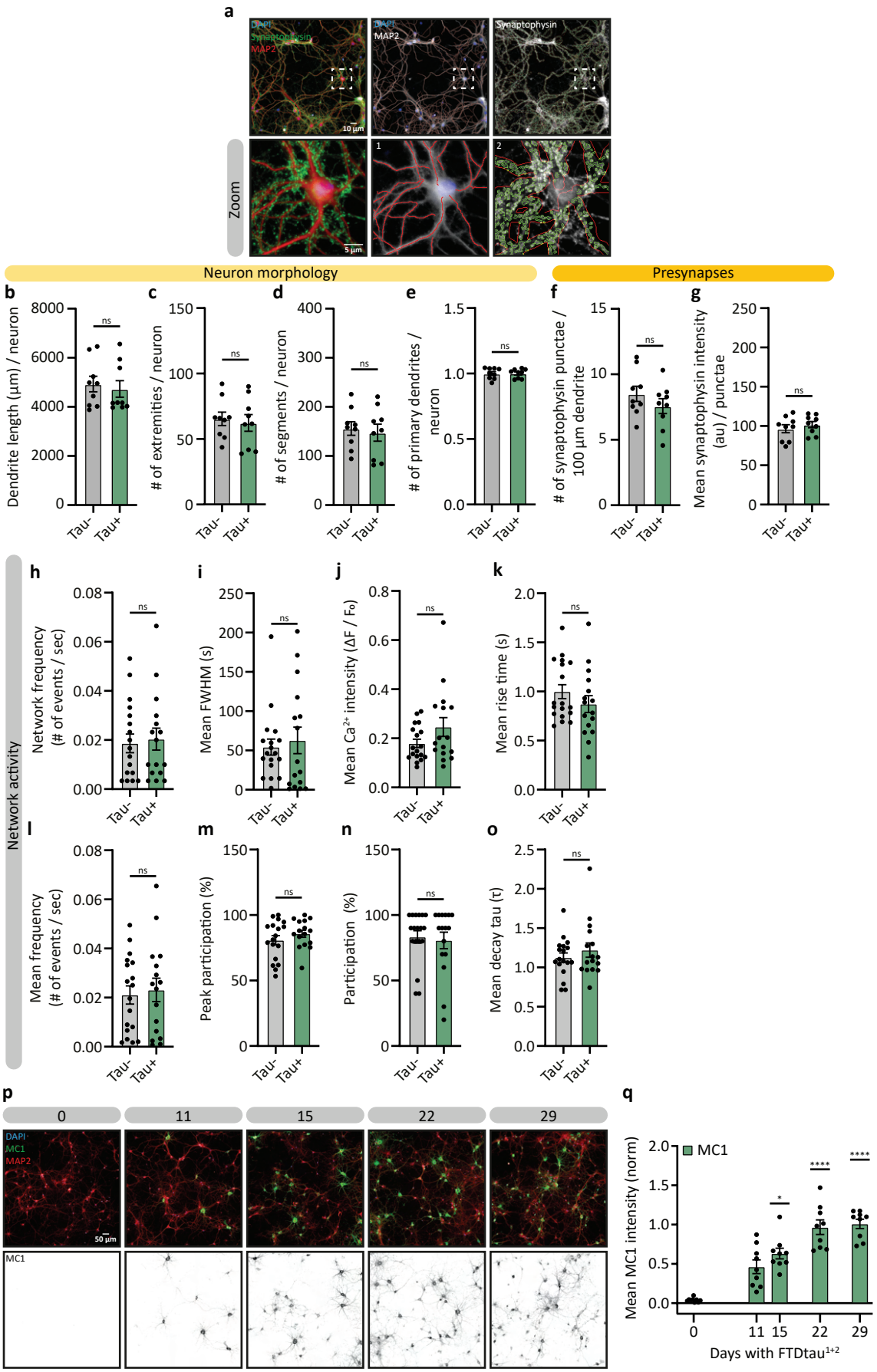

1198 **Extended Data Fig.1: Tau aggregation does not alter neuronal morphology, viability and**
1199 **network activity. a** Representative high-content microscopy images showing the workflow for
1200 assessing neuron and pre-synapse morphology based on immunofluorescence staining of the
1201 dendrite marker MAP2 (red, grey) and the pre-synapse marker synaptophysin (green, grey)
1202 analysed at day 15. Nuclei were visualised by DAPI (blue). The zoomed regions are indicated
1203 by dashed white squares. The detection of dendrites is based on the MAP2 signal (red traces,
1204 1) and pre-synapses (yellow outline, 2) are defined using synaptophysin punctae within the
1205 dendrite region (red outline, 2). **b-g** Quantification of neuron and pre-synapse morphology in
1206 tau- or tau+ neurons analysed at day 15, including dendrite length (**b**), number of extremities
1207 (**c**), number of segments (**d**), and number of primary dendrites (**e**), normalised to neuron
1208 number. Pre-synaptic analysis includes pre-synapse density (**f**) and synaptophysin intensity
1209 (**g**) normalised to dendrite length. N=3 and n=9. A Mann-Whitney test (**b**) and a nested t-test
1210 (**c-g**) were used. **h-o**: Quantification of network activity in tau- or tau+ neuronal networks using
1211 calcium imaging analysed at day 15 including network frequency (**h**), mean full width half
1212 maximum (FWHM) (**i**), mean calcium intensity (**j**), mean rise time (**k**), mean frequency (**l**), peak
1213 participation (**m**), participation (**n**) and mean decay tau (**o**). Single datapoints represent
1214 recordings from 10 neurons per field of view. N=3 and n=18 (tau-) or 16 (tau+). A Mann-
1215 Whitney test (**h-k, n, o**) and a nested t-test (**l, m**) were used. **p** Representative high-content
1216 microscopy images at different FTDtau$^{1+2}$ exposure durations as indicated. Neurons were
1217 immunostained for the pathological tau marker MC1 (green) and MAP2 (red) and nuclei were
1218 visualised by DAPI (blue). MC1 channel is shown in greyscale. **q** Quantification of mean MC1
1219 immunofluorescence intensity normalized to 29 days FTDtau$^{1+2}$ exposure (1) and
1220 untransduced (0). Single datapoints represent one well. N=3 and n=9 for all FTDtau$^{1+2}$-
1221 exposures. A Kruskal-Wallis test followed by a Dunn's post-hoc test was used. Single data
1222 points represent one well (**b-g, q**). Data are presented as mean ± s.e.m. *P*-values are
1223 indicated: **P* < 0.05, *****P* < 0.0001 and ns: not significant.

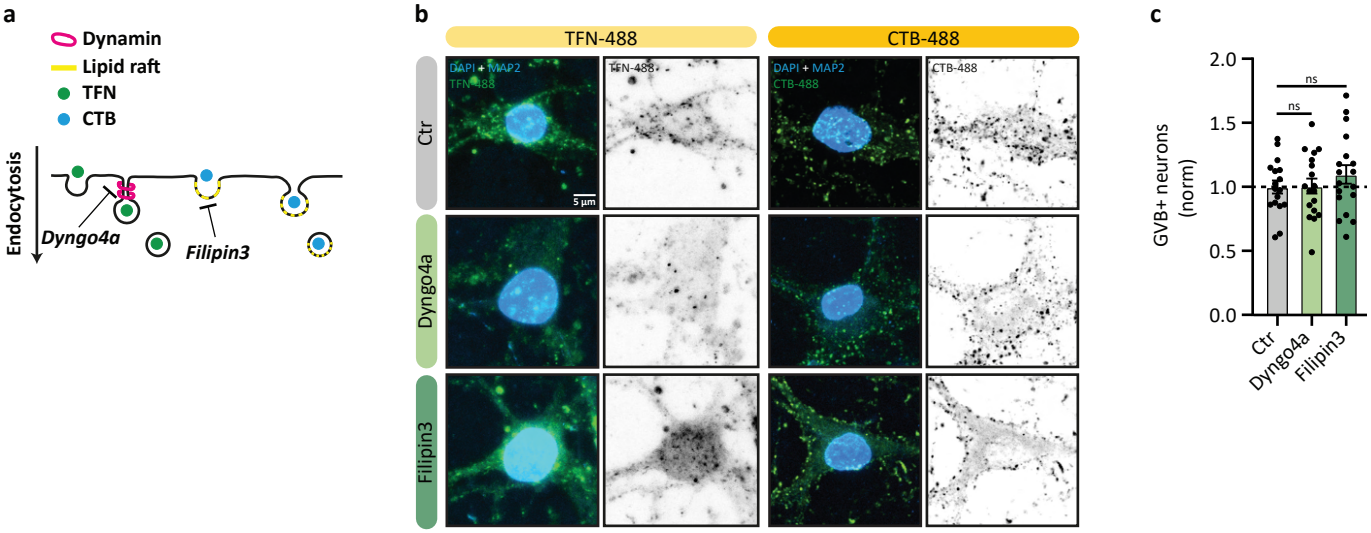


1224 **Extended Data Fig.2: Inhibition of endocytosis does not affect the formation of GVBs.**
1225 **a** Schematic of interventions used to block dynamin- and lipid raft dependent endocytosis. **b**
1226 Representative confocal images of tau+ neurons analysed at day 15. Neurons were left
1227 treated without or with the dynamin inhibitor Dyngo4a or the lipid raft inhibitor Filipin3 for 48h.
1228 The neurons were incubated for 23h with transferrin-488 (TFN-488) or for 30 min with Cholera
1229 Toxin Subunit B (CTB-488) and immunostained for MAP2 (blue). Nuclei were visualised by
1230 DAPI (blue). Separate channels are shown in greyscale. **c** Quantification of the percentage of
1231 pPERK+ GVB+ neurons upon Dyngo4a or Filipin3 treatment, normalised to untreated. Single
1232 datapoints represent one well. N=3 and n=17 (Ctr), 18 (Dyngo4a) and 18 (Filipin3). A nested
1233 one-way ANOVA test followed by a Dunnett's post-hoc test was used. Data are presented as
1234 mean ± s.e.m. *P*-values are indicated: ns: not significant.

# Extended Data Fig.3

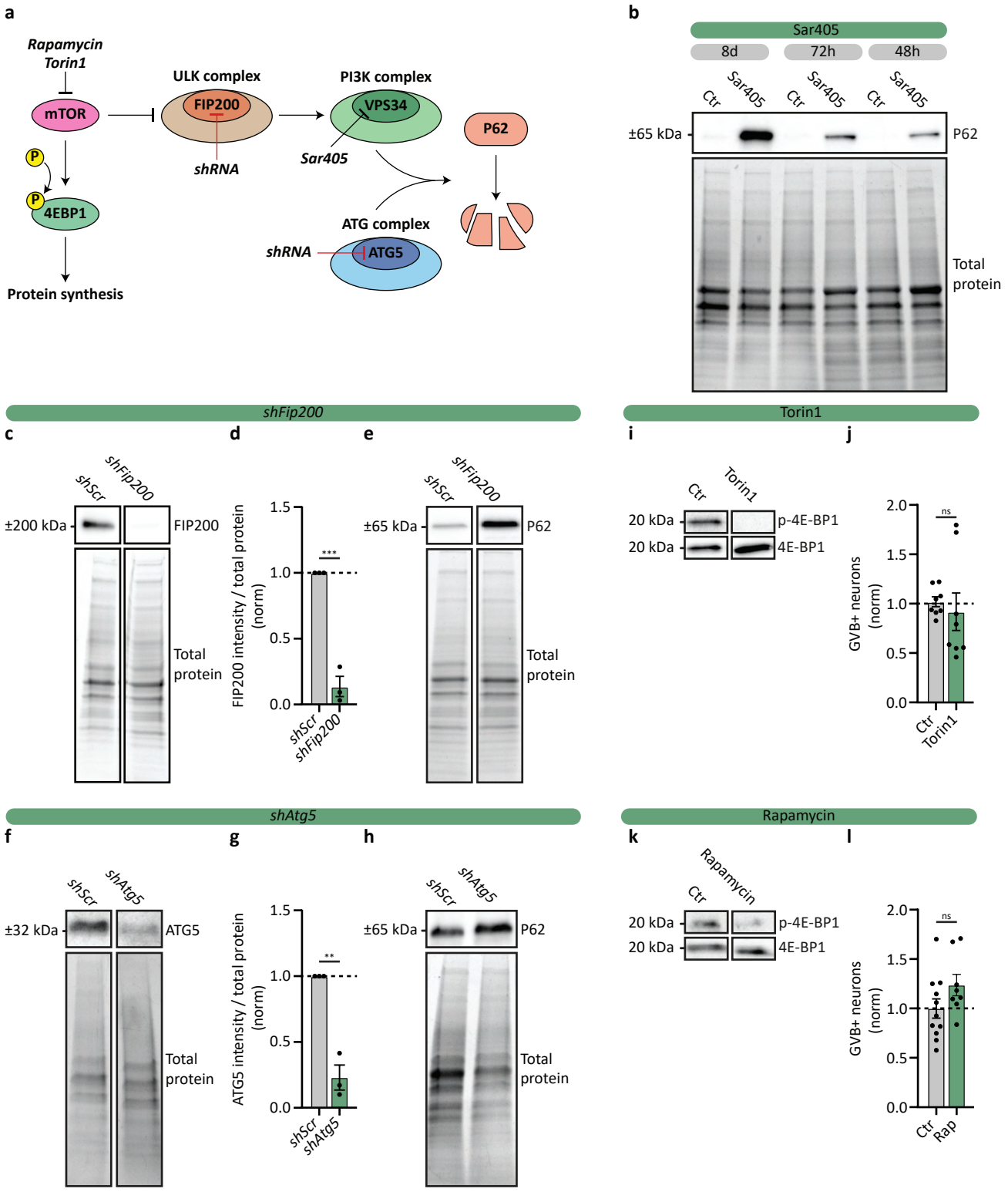

1235 **Extended Data Fig.3: Validation of autophagy interventions. a** Schematic of interventions
1236 used to block mTOR-dependent autophagy. **b** Representative western blot of P62 of neurons
1237 treated without or with Sar405 for 8d, 72h or 48h, analysed at day 15. **c** Representative
1238 western blot of FIP200 of neurons transduced with *shScr* or *shFip200* 8d before analysis at
1239 day 15. **d** Quantification of FIP200 intensity over total protein upon *Fip200* knock-down (KD)
1240 normalised to *shScr*. Single datapoints represent individual experiments. N=3. An unpaired t-
1241 test was used. **e** Representative western blot of P62 of neurons transduced with *shScr* or
1242 *shFip200* 8d before analysis at day 15. **f** Representative western blot of ATG5 of neurons
1243 transduced with *shScr* or *shAtg5* 8d before analysis at day 15. **g** Quantification of ATG5
1244 intensity over total protein upon *Atg5* KD normalised to *shScr*. Single datapoints represent
1245 individual experiments. N=3. An unpaired t-test was used. **h** Representative western blot of
1246 P62 of neurons transduced with *shScr* or *shAtg5* 8d before analysis at day 15. **i, k**
1247 Representative western blot of p-4E-BP1 and 4E-BP1 of neurons treated without or with
1248 Torin1 (**i**) or rapamycin (**k**) for 48h analysed at day 15. **j, l** Quantification of the percentage of
1249 pPERK+ (**j**) or CK1δ+ (**l**) GVB+ neurons upon 48h of Torin1 (**j**) or rapamycin (**l**) treatment
1250 normalised to untreated per timepoint analysed at day 15. Single datapoints represent one
1251 well. N=3 and n=8 and 8 (Torin1) or n=11 and 8 (rapamycin), Ctr and Torin1 or rapamycin,
1252 respectively. A nested t-test was used (**j, l**). Data are presented as mean ± s.e.m. *P*-values
1253 are indicated: $^{**}P < 0.01$, $^{***}P < 0.001$ and ns: not significant.

# Extended Data Fig.4

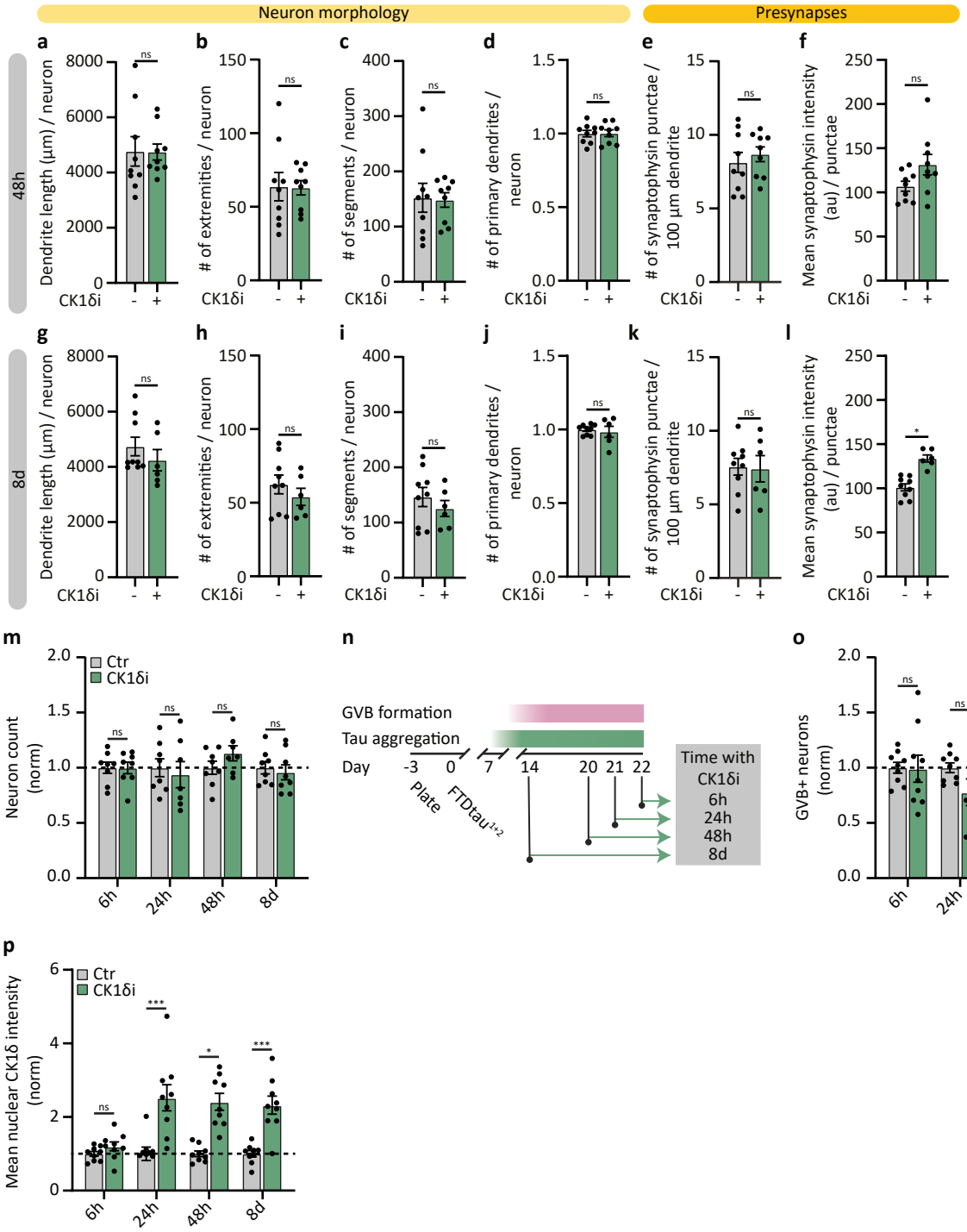

1254 **Extended Data Fig.4: CK1δ inhibition does alter neuronal morphology. a-l** Quantification
1255 of neuron and pre-synapse morphology of tau+ neurons treated without or with CK1$\delta_i$ for 48h
1256 or 8d analysed at day 15. Dendrite length (**a, g**), number of extremities (**b, h**), number of
1257 segments (**c, i**) and number of primary dendrites (**d, j**) were normalised to number of neurons.
1258 Number of pre-synapses (**e, k**) was normalised to dendrite length and the intensity of
1259 synaptophysin was measured within single pre-synapses (**f, l**). N=3, n=9 and 9 (48h), 9 and 6
1260 (8d), for Ctr and CK1$\delta_i$, respectively. A nested t-test (**a-f, h-l**) and a Mann-Whitney test (**g**)
1261 were used. **m** Quantification of tau+ neuron number upon CK1$\delta_i$ treatment for 6h, 24h, 48h or
1262 8d analysed at day 15 normalised to untreated per timepoint. N=3 and n=8 and 8 (6h), 8 and
1263 8 (24h), 8 and 7 (48h), 8 and 8 (8d), for Ctr and CK1$\delta_i$, respectively. A nested t-test was used.
1264 **n** Schematic of the timeline of CK1$\delta_i$. **o, p** Quantification of the percentage of pPERK+ GVB+
1265 neurons (**o**) and mean nuclear CK1δ intensity (**p**) upon CK1$\delta_i$ treatment analysed at day 22
1266 normalised to untreated per timepoint. N=3 and n=9. A Mann-Whitney test (24h; **p**) and a
1267 nested t-test (the rest) was used. Single data points represent one well (**a-l, m, o, p**). Data are
1268 presented as mean ± s.e.m. *P*-values are indicated: *$P < 0.05$, ***$P < 0.001$, ****$P < 0.0001$
1269 and ns: not significant.

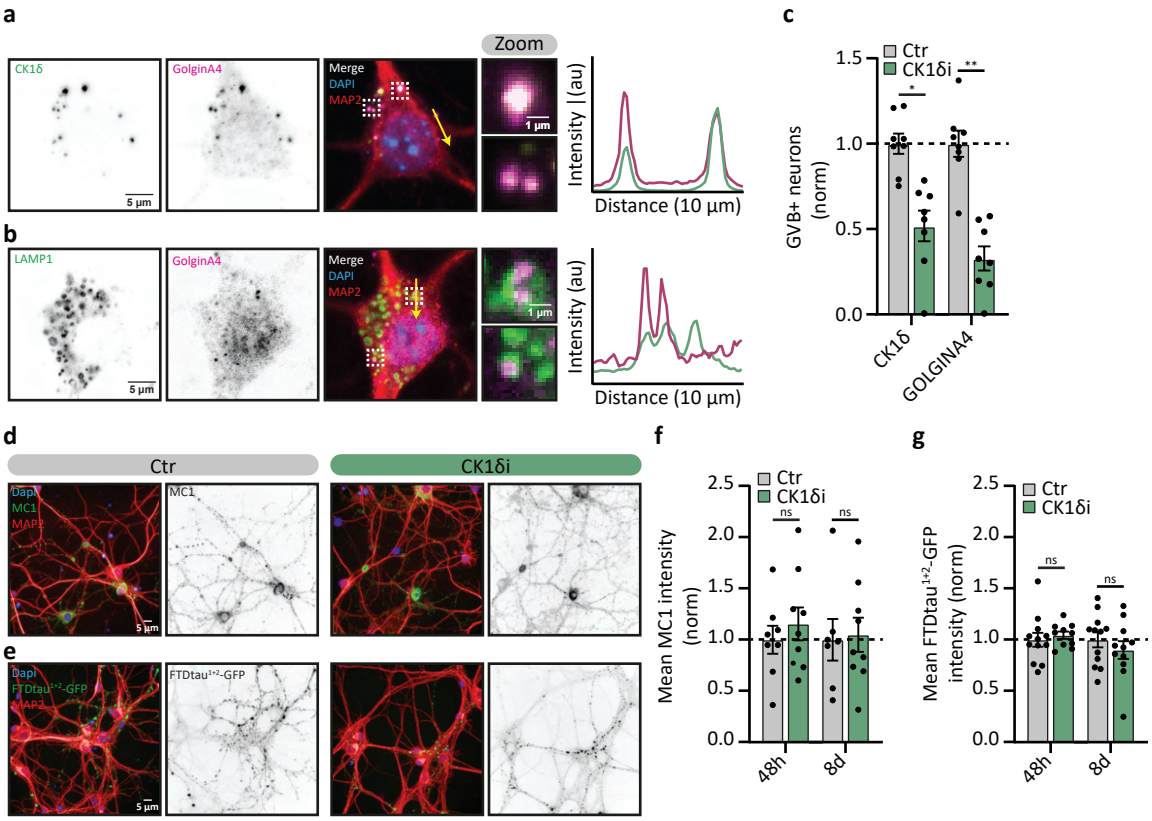


**Extended Data Fig.5: CK1δ does not affect GVB detection or tau pathology. a, b** Representative confocal images of tau+/GVB+ neurons analysed on day 22. Neurons were immunostained for the GVB markers CK1δ (green) and GOLGINA4 (magenta) (**a**), the lysosomal membrane marker LAMP1 (green) and GOLGINA4 (magenta) (**b**) and the dendrite marker MAP2 (red). The zoomed regions are indicated by dashed white squares and the yellow arrow represents the location of the line intensity profiles. **c** Quantification of the percentage of CK1δ+ or GOLGINA4+ GVB+ neurons upon 48h of CK1$\delta_i$ treatment analysed at day 22 normalised to untreated per GVB-marker. N=3, n=8. A nested t-test was used. **d, e** Representative high-content microscopy images of FTDtau$^{1+2}$- (**d**) or FTDtau$^{1+2}$-GFP-transduced (green) (**e**) neurons treated without or with CK1$\delta_i$ for 48h and analysed at day 15. Neurons were immunostained for the pathological tau marker MC1 (green) (**d**) and MAP2 (red). **f** Quantification of mean MC1 immunofluorescence intensity upon CK1$\delta_i$ for 48h or 8d normalised to untreated control. N=3 and n=8 and 9 (48h), 7 and 9 (8d), for Ctr and CK1$\delta_i$, respectively. A nested t-test was used. **g** Quantification of mean FTDtau$^{1+2}$-GFP intensity upon CK1$\delta_i$ for 48h or 8d normalised to untreated control. Single data points represent one well. N=4 and n=12 and 10 (48h), 12 and 11 (8d), for Ctr and CK1$\delta_i$, res ectively. A nested t-test was used. Nuclei were visualised by DAPI (blue) and separate channels are shown in greyscale (**a, b, d, e**). Single data points represent one well (**c, f, g**). Data are presented as mean ± s.e.m. *P*-values are indicated: **P* < 0.05, ***P* < 0.01 and ns: not significant.

# Extendetd Data Fig.6

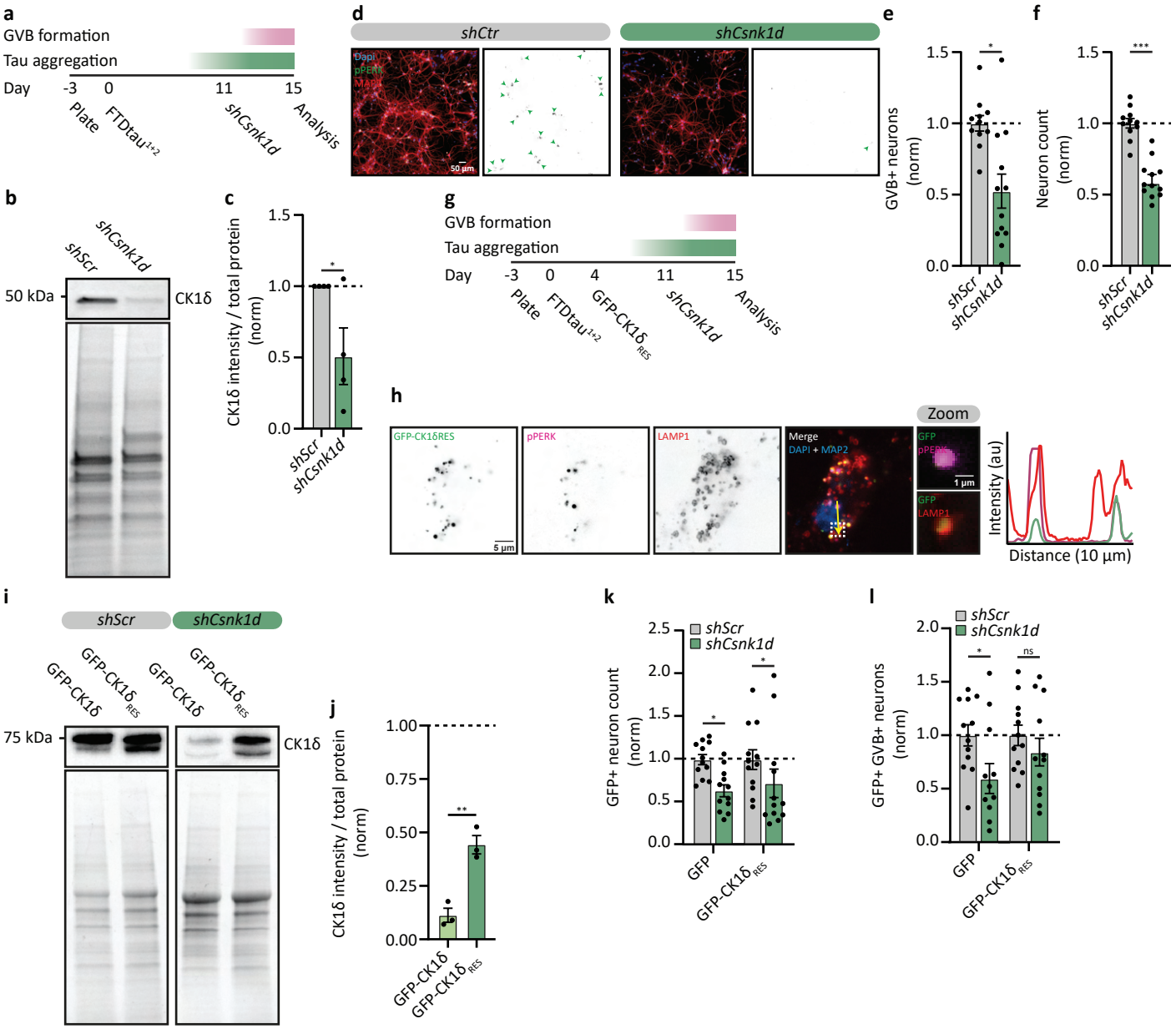

1289 **Extended Data Fig.6: CK1δ knock-down reduces GVB formation. a** Schematic of the
1290 timeline of CK1δ knock-down (KD). **b** Representative western blot of CK1δ of neurons
1291 transduced with *shScr* or *shCsnk1d* 4d before analysis at day 15. **c** Quantification of CK1δ
1292 intensity over total protein upon *Csnk1d* KD normalised to *shScr*. Single datapoints represent
1293 individual experiments. N=4. An unpaired t-test was used. **d** Representative high-content
1294 microscopy images of tau+ neurons transduced with *shScr* or *shCsnk1d* 4d before analysis at
1295 day 15. Neurons were immunostained for the GVB marker pPERK (green) and the dendrite
1296 marker MAP2 (red). Green arrowheads indicate GVB+ neurons. **e, f** Quantification of the
1297 percentage of pPERK+ GVB+ neurons (**e**) or neuron number (**f**) of tau+ neurons upon 4d of
1298 *Csnk1d* KD normalised to *shScr*. Single datapoints represent one well. N=4 and n=11 and 12,
1299 for *shScr* and *shCsnk1d*, respectively. A nested t-test (**e, f**) was used. **g** Schematic of the
1300 timeline of CK1δ KD and rescue. **h** Representative confocal images of tau+/GVB+ neurons
1301 analysed at day 22. Neurons were transduced with GFP-CK1$\delta_{RES}$ which also localised to
1302 GVBs. The neurons were immunostained for pPERK (magenta), the lysosomal membrane
1303 marker LAMP1 (red) and MAP2 (blue). The zoomed region is indicated by a dashed white
1304 square and the yellow arrow represents the location of the line intensity profile. **i**
1305 Representative western blot of CK1δ of neurons transduced with GFP-CK1δ or GFP-CK1$\delta_{RES}$
1306 at day 4 and subsequently transduced with either *shScr* or *shCsnk1d* at day 11 and analysed
1307 at day 15. **j** Quantification of CK1δ intensity over total protein upon *Csnk1d* normalised to
1308 *shScr* per group and analysed at day 15. GFP-CK1$\delta_{RES}$ shows a partial rescue of CK1δ protein
1309 levels. Single datapoints represent individual experiments. N=3. An unpaired t-test was used.
1310 **k, l** Quantification of the number of GFP+ neurons (**k**) or the percentage of pPERK+ GVB+
1311 neurons transduced with GFP or GFP-CK1$\delta_{RES}$ upon *Csnk1d* KD analysed at day 15 and
1312 normalised to *shScr* treated neurons per group. N=4 and n=12. Nuclei were visualised by
1313 DAPI (blue) and separate channels are shown in greyscale (**d, h**). Data are presented as
1314 mean ± s.e.m. *P*-values are indicated: **P* < 0.05, ***P* < 0.01, ****P* < 0.001 and ns: not
1315 significant.

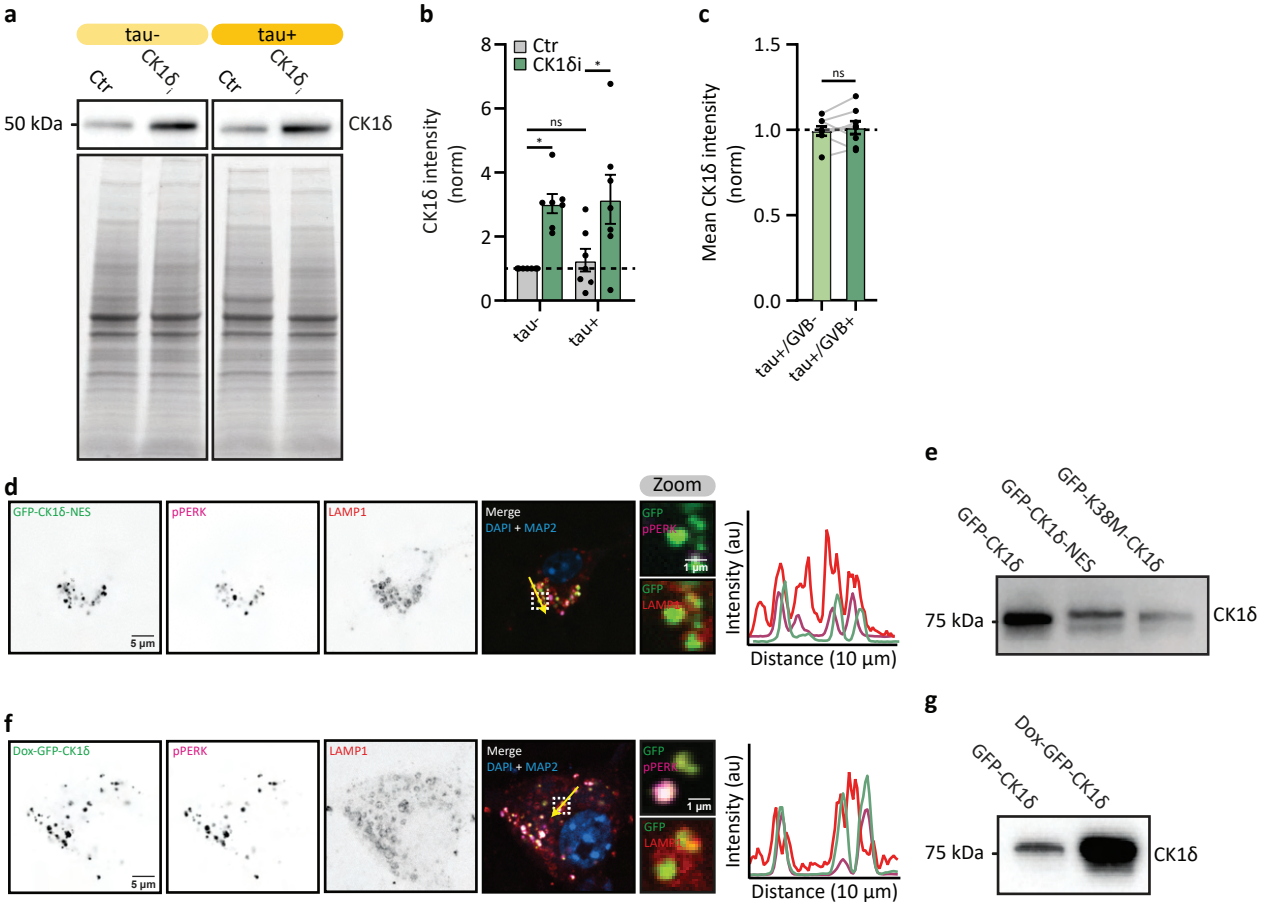


**Extended Data Fig.7: Tau aggregation does not increase CK1δ levels. a** Representative western blot of CK1δ of tau- or tau+ neurons that were treated without or with CK1δ$_i$ for 48h. **b** Quantification of CK1δ intensity of tau- or tau+ neurons that were treated without or with CK1δ$_i$ for 48h and analysed at day 15. Single datapoints represent individual experiments. N=7. A two-way ANOVA followed by a Tukey's post-hoc test was used. **c** Quantification of somatic CK1δ intensity in tau+/GVB- and tau+/GVB+ (pPERK based) neurons, excluding the GVB-area, normalised to tau+/GVB- neurons. Single data points represent one well. N=3 and n=8. A paired t-test was used. **d, f** Representative confocal images of tau+/GVB+ neurons analysed at day 22. Neurons were transduced with GFP-CK1δ-NES (**d**) or Dox-GFP-CK1δ and treated with Dox for 48h (**f**). The neurons were immunostained for the GVB marker pPERK (magenta), the lysosomal membrane marker LAMP1 (red) and the dendrite marker MAP2 (blue). Nuclei were visualised by DAPI (blue). Separate channels are shown in greyscale. The zoomed regions are indicated by dashed white squares and the yellow arrow represents the location of the line intensity profiles. **e, g** Representative western blots of CK1δ of neurons transduced with GFP-CK1δ (**e**, **g**), GFP-CK1δ-NES (**e**), GFP-CK1δ-K38M (**e**) or Dox-GFP-CK1δ and treated with Dox for 48h (**g**) and analysed at day 15. Data are presented as mean ± s.e.m. *P*-values are indicated: *$P < 0.05$ and ns: not significant.

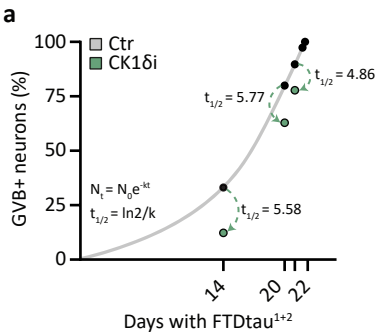


**Extended Data Fig.8: GVBs are stable structures. a** Visualisation of GVB half-life ($t_{1/2}$) based on the polynomial equation obtained from Fig. 1h ($y = 0.05x^2 - 0.3x + 0.2$) to calculate the expected amount of GVB+ neurons after different exposure periods to tau aggregation (grey line) and the observed amount of GVB+ neurons upon 24h, 48h and 8d of CK1$\delta_i$ (Supplementary Fig. 4o). Assuming an exponential decay ($N_t=N_0e^{-kt}$ and $t_{1/2}=ln2/k$), $t_{1/2}$ was calculated using the ratio of expected over observed amount of GVB+ neurons upon CK1$\delta_i$. The green arrows indicate the difference in expected and observed amount of GVB+ neurons per timepoint.

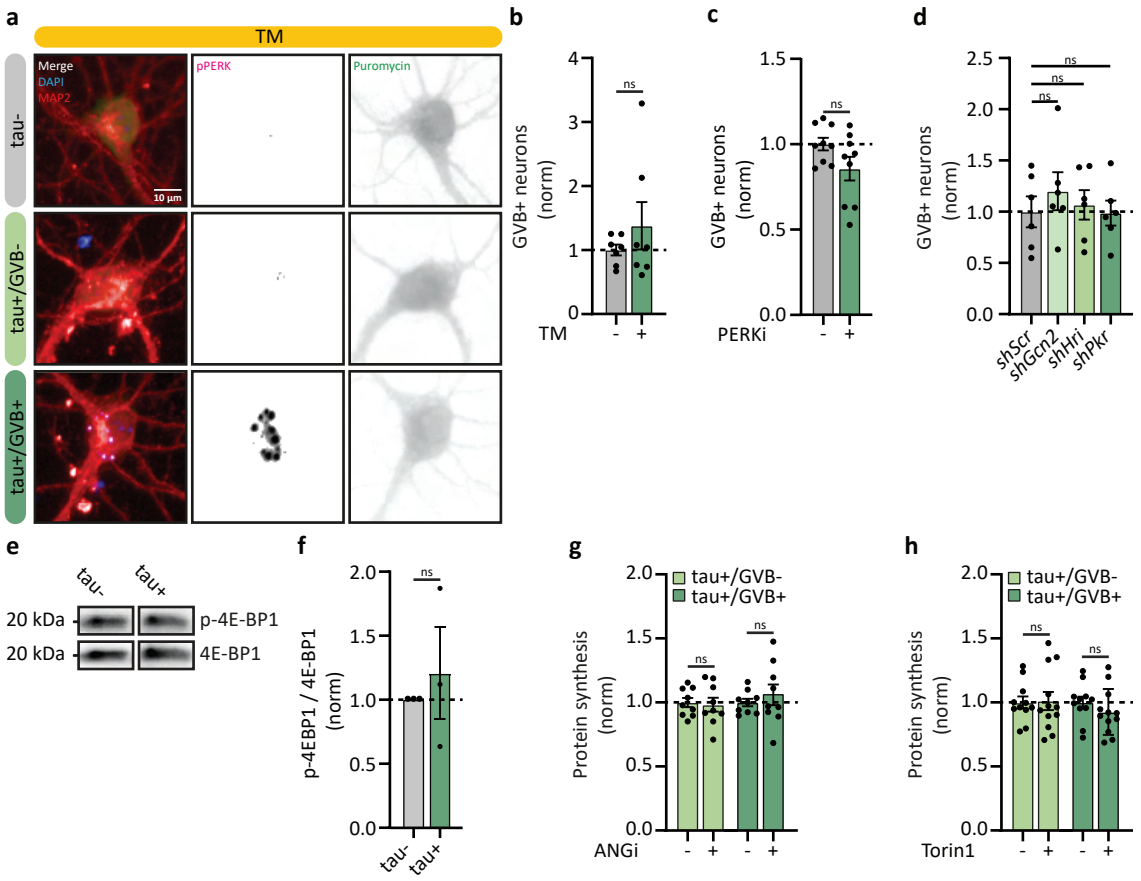


**Extended Data Fig.9: GVB formation and regulation does not depend on transient stress pathways. a** Representative high-content microscopy images showing tau-, tau+/GVB- and tau+/GVB+ neurons treated with TM for 24h analysed at day 22. Neurons were treated for 15min with puromycin and were immunostained for puromycinilated proteins (green), the dendrite marker MAP2 (red) and the GVB marker pPERK (magenta). Nuclei were visualised by DAPI (blue). Separate channels are shown in greyscales. **b, c** Quantification of the percentage of CK1δ+ (**b**) or pPERK+ (**c**) GVB+ neurons upon TM (**b**) or PERK$_i$ (**c**) treatment for 48h analysed at day 15 normalised to untreated. N=3 and n=7 (TM; **b**), 9 (PERKi; **c**). A Mann-Whitney test (**b**) and nested t-test (**c**) were used. **d** Quantification of the percentage of CK1δ+ GVB+ neurons after 8d of knock-down of the EIF2AK proteins *Gcn2* (*Eif2ak4*), *Pkr* (*Eif2ak2*) and *Hri* (*Eif2ak1*) normalised to neurons transduced with the *shScr*. N=3 and n=6. A nested one-way ANOVA followed by a Dunnett's post-hoc test was used. **e** Representative western blot of p-4E-BP1 and 4E-BP1 of tau- or tau+ neurons analysed at day 15. **f** Quantification of p-4E-BP1 over 4E-BP1 intensity of tau+ neurons normalised to tau- analysed at day 15. N=3. An unpaired t-test was used. **g, h** Quantification of puromycin intensity as a measure for *de novo* protein synthesis in tau-, tau+/GVB- and tau+/GVB+ (pPERK based) neurons treated with angiogenin inhibitor (ANG$_i$, **g**) or Torin1 (**h**) for 24h analysed at day 22 normalised to untreated per group. N=3 and n=9. A nested t-test (**g, h**) was used. Single datapoints represent one well (**b-d, g, h**). Data are presented as mean ± s.e.m. *P*-values are indicated: ns: not significant.

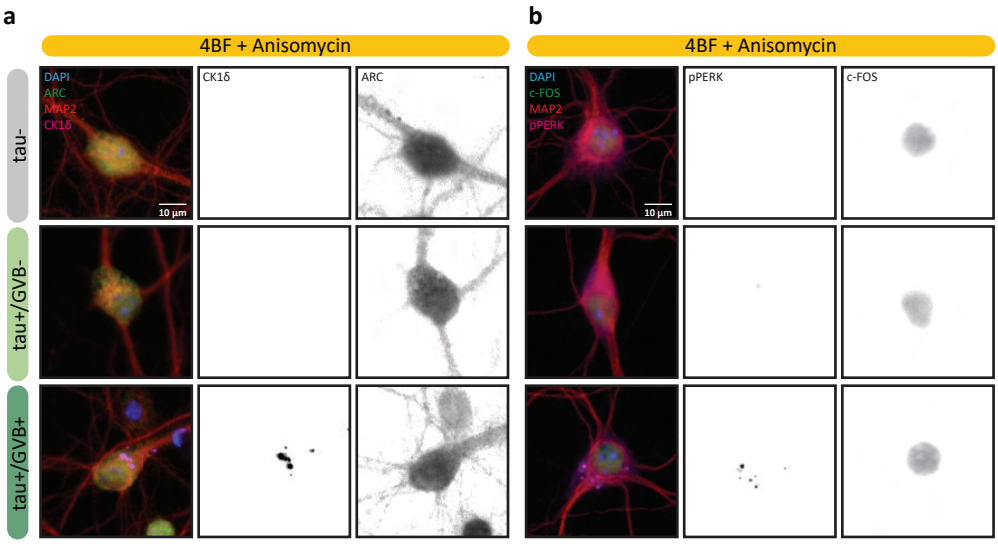


**Extended Data Fig.10: LTP-dependent induction of immediately early genes (IEGs) is dependent on protein synthesis**. **a, b** Representative high-content microscopy images of tau-, tau+/GVB- and tau+/GVB+ neurons treated with anisomycin prior to treatment with 4BF (see Methods) for 4h. Neurons were immunostained for IEGs ARC (**a**) (green) or c-FOS (**b**) (green), the dendrite marker MAP2 (red) and the GVB markers CK1δ (magenta) (**a**) or pPERK (magenta) (**b**). Nuclei were visualised by DAPI (blue). Separate channels are shown in greyscales.

1368 **Supplementary Video 1: GVBs are stable, dynamic structures.** Representative live
1369 imaging of a tau+ neuron transduced with GFP-CK1δ (grey) and imaged at day 21. An image
1370 was taken every 20 min for the duration of 9.20h. Although GVBs very rarely appeared or
1371 disappeared, this example shows a GVB disappearing (red arrow) and one appearing (black
1372 arrow).